Cement and Concrete Composites 143 (2023) 105239

Contents lists available at ScienceDirect

Cement and Concrete Composites

journal homepage: www.elsevier.com/locate/cemconcomp

# Assessment of impact resistance recovery in Ultra High-Performance Concrete through stimulated autogenous self-healing in various healing environments

Niranjan Prabhu Kannikachalam [a,b,*], Paula Sofia Marin Peralta [a], Didier Snoeck [c], Nele De Belie [b], Liberato Ferrara [a,**]

[a] Department of Civil and Environmental Engineering, Politecnico di Milano, Italy
[b] Department of Structural Engineering and Building Materials, Magnel-Vandepitte Laboratory, Ghent University, Belgium
[c] Building, Architecture and Town Planning (BATir) Department, Université Libre de Bruxelles, Belgium

ARTICLE INFO

*Keywords:*
Self-healing
Impact test
Ultra high-performance concrete
Crystalline admixture
Autogenous self-healing

ABSTRACT

Ultra High-Performance Concrete (UHPC) is widely acknowledged for its remarkable mechanical properties, owing to its compact microstructure. The response of UHPC to impact forces plays a vital role in ensuring the safety and longevity of structures, specifically in protective buildings, high-performance pavements and offshore concrete structures. In this context, this paper reports on an experimental investigation aimed at assessing the effects of stimulated autogenous self-healing of UHPC on the recovery of its performance under impact loadings. Drop weight tests were performed on UHPC slabs, with a 10 kg heavy impactor dropped from the height of 1 m on the centre of the specimens. Specimens were pre-cracked by repeated impacts up to 40% of their pre-determined capacity. Pre-cracked specimens were exposed to different healing conditions, water submersion, 95% ± 5% RH, and wet/dry cycling (12/12 h) either in water or in a NaCl solution. Self-healing was evaluated through rebound height, elastic stiffness recovery, natural frequency, and laser displacement measurements. High-speed cameras and Digital Image Correlation were used to capture rebound height and crack formation. Performance was assessed at time 0, pre-damaging, 1, 2, and 4 months. After the healing period, all specimens were tested to failure. Specimens exhibited an increasing healing efficiency when moving from 95% ± 5% RH, over wet/dry cycling, to submerged conditions. Specimens healed continuously under submerged conditions exhibited a complete closure of surface cracks (50–150 μm) and an 80% recovery in natural frequency. Furthermore, they showed a more than 10% increase in stiffness and energy dissipation capacity after four months of healing.

## 1. Introduction

Ultra High-Performance Concrete (UHPC) is a broad category of advanced cement-based materials that has been gaining popularity in recent years due to its exceptional mechanical properties, durability and resistance to various environmental exposures. UHPC is a cementitious composite whose mix-design is generally characterized by a high dosage of binder, incorporating cement and different types of supplementary cementitious materials, fine aggregates (coarse aggregates are excluded because of the required matrix compactness), steel or synthetic fibres, which have the primary purpose of tempering the inherent brittleness, chemical admixtures, primarily superplasticizers which guarantee the required workability in view of the generally employed very low water/binder ratio, and other additives. One of the key components that contributes to the exceptional mechanical properties of UHPC is the addition of fibres. As a matter of fact, thanks to a micromechanics-based design of the mix composition, which makes the fibre pull-out energy at the location of an already formed crack higher than the energy required to form a new cracked surface further away from the existing one(s), a stable multiple-cracking behaviour is obtained after the first cracking and before the unstable localization of a single major crack [1]. The extent to which this behaviour takes place, clearly depends on matrix

* Corresponding author.Department of Civil and Environmental Engineering, Politecnico di Milano, Italy.
** Corresponding author.
*E-mail addresses:* niranjanprabhu.kannikachalam@polimi.it (N.P. Kannikachalam), liberato.ferrara@polimi.it (L. Ferrara).

https://doi.org/10.1016/j.cemconcomp.2023.105239
Received 29 April 2023; Received in revised form 5 August 2023; Accepted 8 August 2023
Available online 12 August 2023

properties and fibre-matrix interaction, including alignment of the fibres with respect to the applied tensile stress. This results into a strain hardening behaviour which allows damage due to mechanical actions (among others) to be spread into multiple tiny and closely spaced cracks rather than being concentrated into a single large crack, which is surely beneficial for structural safety, serviceability and durability [2,3]. In this context, it is evident that fibres play an important role in improving also the impact resistance of UHPC by preventing the formation of large cracks and their unstable localization and by providing a mechanism for energy dissipation which reduces the amount of damage suffered by the material. As said above, fibres in UHPC help to (re)distribute the stress throughout the material rather than allowing it to concentrate in one area, which can lead to catastrophic failure. The type of fibres and its quantity used in UHPC can have a significant influence on its impact resistance. By incorporating polymer and steel fibres into concrete, Bindiganavile and Banthia [4–6] proved that its resistance to impact loading is enhanced and its flexural strength is increased. Furthermore, they explored the influence of various factors, including pull-out strength, types of fibres, damage patterns, and fractured surfaces, using quasi-static loading rates of $3.3 \times 10^{-5}$ m/s and impact loading rates of 2 and 3 m/s. It was shown that UHPC, when subjected to impact, is capable of dissipating significantly more energy than conventional FRC with polymeric or steel fibre. This can be attributed to the advantageous combination of a high-strength matrix and a high-volume fraction of steel fibre (0.5%–6%), which creates a synergistic effect [6,7]. As a result, UHPC is highly recommended for use in structures that may be subjected to blast or impact loading. Such structures may include gas tanks, nuclear reactor containment shields, defense shelters and bunkers, heavy-duty runways, crash barriers, as well as military and strategic structures designed to withstand attacks with explosives and impact loading.

Despite its impressive mechanical properties, UHPC can as well suffer cracking from causes other than mechanical loading, including restrained shrinkage, especially autogenous due to the peculiar mix composition, restrained thermal deformations, accidental extreme loading events, and, though less susceptible than ordinary (reinforced) concrete, it can suffer damage from environmental actions including freeze-thaw and thermal cycles and other chemical attacks [8,9]. However, its unique composition, which, as remarked above, features high dosage of binder (also able to develop pozzolanic and latent hydraulic activity) and low water/binder ratios, allow for sensible autogenous self-healing. Hence, the cracks can close or heal over time without external intervention when moisture is present to activate the aforesaid reactions and the other self-healing mechanisms, including carbonation. As known, the main mechanisms involved in autogenous self-healing are the hydration of unhydrated cement particles, pozzolanic/latent hydraulic activity of supplementary cementitious materials, and diffusion of calcium and silicates accompanied by the precipitation of calcium carbonate [10,11]. The effectiveness of the autogenous self-healing in UHPC can be stimulated by means of tailored additions, including e.g., crystalline admixtures eventually in synergy with nano-particles. Crystalline admixtures show promising capabilities in promoting autogenous self-healing mechanisms within concrete structures. When these admixtures are added to the concrete mix, they interact with cement and water during the hydration process, leading to the formation of altered calcium silicate hydrates and insoluble pore-blocking material. As a result, the concrete gains improvement in healing cracks. The incorporation of crystalline admixtures encourages the growth of ettringite on the surfaces of cracks. This ettringite not only aids in the healing of cracks but also forms a network structure that enhances the crystallization of $CaCO_3$. Moreover, when used in conjunction with fibres and expansive agents, crystalline admixtures demonstrate an excellent synergetic effect [12–15]. It is furthermore enhanced by a more extended healing period and with abundant water availability [14–22]. Water is critical in autogenous healing as it is a necessary factor for chemical reactions and a medium for transporting fine particles. Research has consistently shown that water immersion is highly beneficial for self-healing, providing an optimal environment for healing responses. Interestingly, some studies have indicated that wet-dry conditions can lead to better healing than continuous water immersion. This improvement is attributed to the availability of abundant $CO_2$ in the air during the dry cycle, which facilitates the easier formation of $CaCO_3$. Regardless, studies indicate that the healing performance is inferior under 95% relative humidity compared to submersion, and wet and dry conditions [10,23–26]. Furthermore, the size of cracks plays a crucial role in crack closure, and autogenous healing can close cracks in the range of a few tens of μm to 100 μm but less than 300 μm. In strain-hardening cementitious material, studies have shown that a typical crack closure was up to 50 μm and practical closure up to 150 μm [2,3,27–30]. This healing depends on the cement content, water to binder ratio, mineral admixtures, age of the cementitious composites, availability of water and total allowed time of healing.

The study of self-healing concrete has emerged as a recent and promising development to address the challenges posed by cracking and degradation in concrete structures. Over time, substantial research work has been conducted on self-healing, exploring various parameters such as self-healing agents, healing environments, age of crack formation, and crack widths. Additionally, some studies have examined the stability of healed cracks and recovery of durability under aggressive conditions like chloride attack, carbonation, sulphate attack, acid attack, water pressure, and freeze-thaw [27,28,31]. Despite these advancements, there remains a notable research gap concerning the evaluation of self-healing concrete under extreme loading conditions, including sustained, impact, cyclic, and high-temperature scenarios. The absence of sufficient knowledge in this area has prompted the development of a new test methodology to assess the impact resistance of advanced materials like Ultra High-Performance Concrete (UHPC). Furthermore, this research also aims to address the knowledge gap concerning the self-healing properties of a well-studied material within our research group in the H2020 ReSHEALience project where different nano-additives, healing environments, crack ages and aggressive conditions were examined. Our previous study on the self-healing performance of UHPC under cyclic loads shows an increase in the stiffness of the concrete matrix and a reduction in the rate of crack opening displacement after healing [3]. Likewise, in this study, it was expected that the impact-resistant capacity of the UHPC material would be restored through self-healing after the impact loading.

The paper is organized as follows: Section 2 describes the materials along with the experimental setup and methods used in this study. Section 3 presents the results of the drop weight tests and non-destructive tests and their analysis to assess the self-healing capacity and its outcomes in terms of recovery of the impact performance. Finally, Section 4 presents the conclusions of this study.

## 2. Materials and methods

### 2.1. UHPC mix design

The specimens needed for the experiment were taken from one-and-half-year-old pre-cast slabs made of UHPC cast at the construction site of a water tank servicing a geothermal power plant (which served as a demonstrator in the already concluded Horizon 2020 project ReSHEALience (GA 760824) [32]. The samples were stored in an open environment prior to being tested; their concrete mix composition is shown in Table 1. Table 2 reports the composition of the employed cement and slag. For this study, twenty-one specimens with dimension 290 × 290 × 40 $mm^3$ (±5 mm) were cut from the six slabs, originally having dimensions equal to 600 × 600 × 40 $mm^3$ (±5 mm), cast for laboratory investigation in moulds alongside with the water tank construction, which results in a significant variation in thickness compared to that of water tank walls. However, which is of great interest since it shows the range of dimensional tolerances obtained and obtainable on a real

**Table 1**
UHPC mix composition.

| Constituents | kg/m$^3$ |
|---|---|
| CEM I 52.5 R | 600 |
| Slag | 500 |
| Water | 200 |
| Steel fibres Azichem Readymesh 200 ® ($l_f$ = 20 mm, $d_f$ = 0.22 mm) | 120 |
| Sand (0–2 mm) | 982 |
| Superplasticizer Glenium ACE 300 ® | 33 |
| Crystalline admixture Penetron Admix ® | 4.8 |

**Table 2**
Composition of the employed cement and slag (contents by % weight).

| Chemical constituent | CEM I | Slag |
|---|---|---|
| $SiO_2$ | 38.9 | 39.2 |
| CaO | 59.7 | 38.9 |
| $Al_2O_3$ | 4.9 | 10.2 |
| MgO | 3.3 | 6.4 |
| $SO_3$ | 3.4 | 1.3 |
| $Mn_2O_3$/MnO | 0.1 | 0.3 |
| $Fe_2O_3$ | 3.5 | 0.4 |
| $TiO_2$ | 0.2 | 0.6 |
| $K_2O$ | 0.2 | 0.8 |
| $Na_2O$ | 0.4 | 0.3 |
| Other | 0.4 | 0.3 |
| Loss on ignition at 1000 °C | 2.5 | 1.2 |

in-situ pre-casting construction worksite. Also, the benefit of using older materials in the self-healing study hydration phase of its constituents is nearly complete, which allows to provide a clearer understanding of its healing capabilities as triggered by the cracking and the ingress of water/moisture from outside. The material properties were extensively studied under static conditions [14,15,17–19,32–35] as part of the H2020 project ReSHEALience: for the intended structural application, the major aim, besides a compression strength of over 100 MPa, was to achieve a tensile strength of 8–10 MPa accompanied by a strain hardening capacity of up to 0.5% and improved durability in harsh environments (XS and XA exposure classes) [15,32,33]. The concrete mix utilized brass-coated straight steel microfibers, measuring 20 mm in length and 0.22 mm in diameter, at a volumetric ratio of 1.5%. This proportion was deemed essential for achieving the desired strain-hardening properties. Additionally, the mix included the crystalline admixture Penetron Admix® at a dose of 0.8% by cement mass as a permeability reducer to stimulate autogenous self-healing. The compressive and flexural strength values at 28 and 84 days were examined for the investigated mixture, showing an average value of 125–165 MPa, and 24–29 MPa, respectively [19]. The specimens' compressive strength of one-year old was around 180 MPa.

### 2.2. Steel fibre dispersion assessment

As is well known, the structural performance of a fibre reinforced concrete element relies on a random uniform dispersion of the fibres. A preliminary check was hence performed on the UHPC slabs employing the method proposed and validated by Ferrara et al. [36–38]. The technique implies measuring the magnetic inductance of the fibre reinforced composite element, using a suitable ferrite probe where a magnetic field is generated through a coil through which an electric current is run. According to a previous study by Al-Obaidi [32], an inductance value of 12.38 μH corresponded to 120 kg/m$^3$ of fibres for the same concrete mixture. Results showed that all slabs feature almost the same average content of fibres, corresponding to the nominal dosage in the mix design with minimal variations, absolutely acceptable in the field (Table 3). The fibre distribution charts are shown in Fig. 1 highlighting a reasonably uniform dispersion inside the large slabs from which the smaller test specimens were cut. In order to eliminate the

**Table 3**
Details of fibre density, thickness of slabs, and healing environment.

| Slabs | Specimen ID | Thickness (mm) | Estimated steel fibre content (kg/m$^3$) |
|---|---|---|---|
| Slab 1 | S1, WD1, RH1, REF1 | 47 ± 2 | 120 |
| Slab 2 | S2, WD2, RH2, WS2 | 36 ± 2 | 119 |
| Slab 3 | S3, WD3, RH3, REF3 | 42 ± 2 | 118 |
| Slab 4 | S4, WD4, RH4, REF4 | 40 ± 2 | 115 |
| Slab 5 | S5, WD5, RH5, WS5 | 43 ± 2 | 120 |
| Slab 6 | WS6 | 34 ± 1 | 116 |

effects due to variations in fibre content and thickness between slabs, a randomized block design was applied in which the four specimens cut from the same slab were assigned to different healing environments after the impact. This approach ensured that any differences in geometry and fibre content would not interfere with the analysis of the healing efficiency. The specimens' ID names started with an acronym for a healing environment (S: submerged, WD: wet/dry - water, WS: wet/dry - NaCl, RH - 95 ± 5% relative humidity) followed by a number which denotes the large slab number from which the specimen was cut. For example, if the specimen is marked as 'WD3′, then the specimen is allocated to a wet/dry healing environment with demineralised water and was taken from slab 3. Reference specimens were marked as REF. Out of four samples in slab 6, only one was selected for the experimental program because two samples were utilized for preliminary work (Prelim) to set up the drop weight tests by changing the weight of the impactor, the height of the drop, the boundary condition of a specimen and also to check working conditions of measuring devices used in the test. An additional sample was kept as a backup in case any allocated specimens failed during the drop weight test.

### 2.3. Drop weight test

The impact performance was investigated using the drop weight test, which was also used to pre-crack and re-crack the specimens during the healing assessment investigation. The test set-up is shown in Fig. 2a: each specimen was clamped at its four corners to the specimen holder, which in turn was firmly secured to a large steel frame. The top frame of the specimen holder was connected to the legs of the machine frame through two impact load cells with a capacity of 89 kN to measure the reaction force under the impact loading (Fig. 2b). A laser device with a resolution range of 2–120 μm was positioned within 120 mm below the specimen along the impact trajectory to measure the specimen's deflection. Fig. 2c shows the laser pointing in the centre of the specimen represented by a "+" sign. Two cameras were also set up at the same level as the laser device to capture the cracking pattern and further elaborate it using Digital Image Correlation (DIC). A 10 kg cylinder impactor with a diameter of 63 mm and a rounded end was attached to an electromagnet, positioned 1 m from the specimen extrados. The impactor was directed to the centre of the specimen through a plexiglass tube attached to the large frame. The rebound height of the impactor was recorded on video at 120 fps (frames per second). A trigger controlled the release of the impactor and the data collected of from the load cells and laser for the following 5 ms. The video recording was started manually before the trigger was released, and the DIC images were taken manually before and after the impact.

The reference specimens underwent repeated impacts, and the results showed that the evolution of the impact load cell readings was similar to the stress-strain curve of UHPC, with the material exhibiting strain-hardening behaviour before experiencing a softening accompanied by the localization of the damage. During the first impact, multiple cracks appeared, followed by additional cracks during subsequent

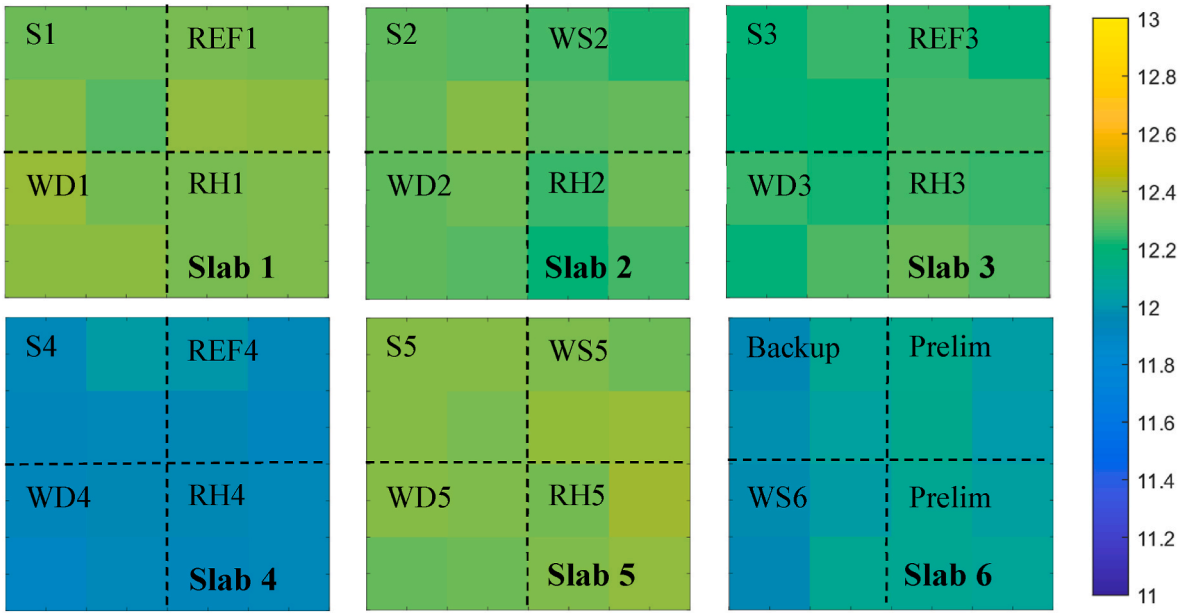


**Fig. 1.** Slabs steel fibre dispersion charts, colour coded for the measured inductance (μH). Slabs were cut into four pieces and allocated to four different healing environments after initial impacts (S: submerged, WD: wet/dry - water, WS: wet/dry - NaCl, RH - 95 ± 5% relative humidity).


**Fig. 2.** a) Impact setup with 10 kg impactor released at the height of 1 m above the centre of a specimen, b) Location of DIC, Laser device and load cell, c) Laser pointing at the centre of the specimen.

impacts. It can be reasonably hypothesised that the hardening response was due to the contribution provided by the fibres in the subsequent impacts. This also has been noticed in DIC images where the number of new cracks formed greatly reduced after the first few impacts and hence the measured hardening, in terms of load cell readings, can be reasonably attributed to the pull-out resistance offered by the fibres crossing the already formed cracks.

The repeated impact testing was continued until the value of the impact reaction force decreased and reached a value systematically lower than the one measured at the first impact or when a maximum of 50 impacts was reached on each specimen. The point where reaction force started systematically decreasing below the value measured at the first impact was considered as the moment when one of the previously formed cracks started to open, and the further opening of this local unstable crack is taken as the failure criterion. Prior to this failure point, a stable multiple crack progression occurred, accompanied by a deflection-hardening response [1,17]. The results indicated that REF1's impact reaction force fell below its first impact value after the 39th impact and continued to decrease thereafter. REF3's impact reaction force dropped below its first impact value after 19 impacts, and REF4's reaction force decreased after 8 impacts (Fig. 3). This difference was a result primarily of the different thickness (47, 42 and 40 mm for REF1, REF3 and REF4 respectively) and, to a much lower extent, of the different fibre distribution in the slabs. The chosen failure criterion was based on several reasons. First, the degree of damage was too extensive for self-healing since the localized crack width exceeded 0.3 mm. Second, surpassing this point would significantly increase the likelihood of material spalling, which would negatively impact laser deflection measurements. Third, although scabbing was present up to this point, impactor penetration had yet to occur. Once this point is reached, the rebound height would not be accurate enough for analysis. As a result, both laser deflection and rebound height readings cannot be considered to define a failure point. Last, any further repeated impacts from this defined failure point would threaten the equipment below the

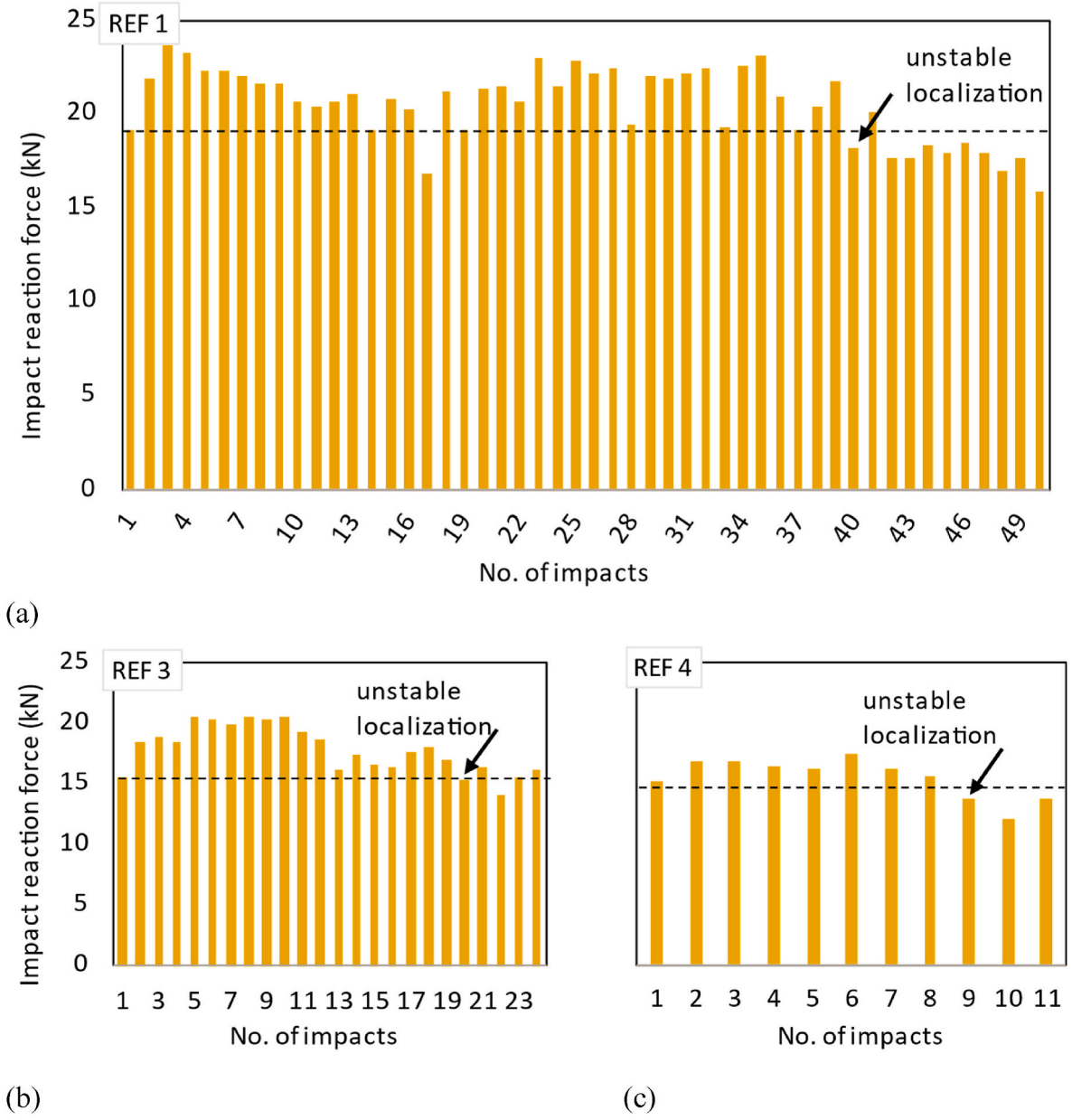


**Fig. 3.** Impact reaction force from a single load cell vs repeated impacts for three different reference specimens (a, b, c). Unstable localization is marked with an arrow (at this stage one crack had opened further), after which a few more repeated impacts were made on the specimen to confirm the strain/deflection softening trend prior to stopping the test on the specimens.

specimens. While the load cell measurements could continue without issues in case of spalling or penetration of the impactor even after unstable localization, they were selected as the basis for defining the failure point.

Based on the above results obtained from the load cell, reading for the REF specimens, pre-cracking was done on the remaining specimens by applying roughly 40% of the impacts needed to reach unstable local crack formation in the weakest specimen (REF4). Specimens from slab 4 and slab 6 were impacted 3 times before healing, while the remaining specimens obtained from other slabs were impacted 6 times since they were more resistant due to the combined effect of thickness and fibre distribution. The specimens were then healed in four different environments: submerged in demineralised water, wet/dry in demineralised water (12/12 h), wet/dry in NaCl aqueous solution (12/12 h), and in moist room at a temperature of 20 ± 2 °C and 95 ± 5% relative humidity (RH), for a maximum of four months. An automated wet/dry procedure was implemented in the laboratory setting, with the aim of drying the specimens at a temperature of 20 ± 2 °C at 60% RH. The demineralised water was replaced every month. The concentration of NaCl was set at 3.3%. The specimens from Slab 4 and Slab 5 were tested for mechanical recovery by undergoing repeated impacts after the first and second months of healing. S4, WD4, and RH4 underwent one impact at each interval, while S5, WD5, and RH5 underwent two impacts. This change in the number of impacts among specimens was due to the same reason as in the pre-cracking i.e. thickness and fibre distribution. Table 4 summarizes the specimen's healing environment and healing period. The term "continuous healing" refers to the process of healing without any repeated damage during a given healing period. On the other hand, "repeated impact/healing" means that the healing process is disrupted at the indicated deadlines by repeated impact damage and then resumed. Both continuous and repeated impact/healing processes hold significance. Continuous self-healing showcases the full potential of the self-healing ability, whereas repeated impact tests, involving multiple incidents, demonstrate the material's ability to heal repeatedly. However, it is essential to consider that the healing potential may reduce over time due to the consumption of readily available free unhydrated cement particles [29,30]. Furthermore, in the future, both continuous healing and repeated healing capabilities could be potentially incorporated into the design of structural members.

After four months, all the healed specimens underwent repeated impact testing with the same conditions as the reference specimens, except for the specimens from Slab 3, which were tested after two months of healing. The load cell readings were used as an indicator to stop the test.

Digital image correlation was used to capture the cracking pattern under repeated impact loading. The camera was focused on the bottom side of the specimen, with the central area of approximately 15 × 15 $cm^2$ in the field of view. The images were taken before and after each impact loading; the image analysis showed multiple cracks on each specimen, and the number of cracks increased with repeated impacts, as shown in Fig. 4. However, the majority of the cracks appeared within the first two or three impacts, and on further impacts, the cracks started to widen slowly. This shows that at that moment, the fibres started to carry the load resulting in strain/deflection hardening behaviour observed through the readings of the impact load cells. The maximum strain during the first impact was about 0.01, and the strain increased for subsequent impacts up to 0.025 at the sixth impact, as can be seen for the specimen WS5 in Fig. 4. The above-mentioned strains are average values over the entire area covered by the DIC system. The formation of multiple cracks is a characteristic feature of fibre-reinforced concrete, which significantly restricts crack width, enabling autogenous self-healing to close the cracks.

**Table 4**
Details of specimens healing environment, healing period and healing type.

| Healing environment | Specimens | Healing time | Healing type |
|---|---|---|---|
| Submerged (S) | S1, S2 | 4 months | Continuous healing |
| | S3 | 2 months | Continuous healing |
| | S4, S5 | 4 months | Repeated impact/healing (1 M & 2 M) |
| Wet/dry – Water (WD) 12/12 h | WD1, WD2 | 4 months | Continuous healing |
| | WD3 | 2 months | Continuous healing |
| | WD4, WD5 | 4 months | Repeated impact/healing (1 M & 2 M) |
| Wet/dry – NaCl (WS) 12/12 h | WS2, WS5, WS6 | 4 months | Continuous healing |
| 95 ± 5% relative humidity (RH) | RH1, RH2 | 4 months | Continuous healing |
| | RH3 | 2 months | Continuous healing |
| | RH4, RH5 | 4 months | Repeated impact/healing (1 M & 2 M) |

The video footage from each impact test was used to compute the rebound height and the restitution coefficient. The rebound height of the impactor was extracted by advancing the video, frame by frame, using iMovie software. A printable ruler had been placed on the transparent plexiglass during the experiment to aid this process. The ratio of the final velocity (v) after collision of the impactor with the specimen, to the initial velocity before collision (u), is defined as the restitution coefficient, as calculated by Eq. (1) where, $h_0$ is the drop height, and $h_f$ is the rebound height.

The final velocity of the impactor is measured immediately after the rebound (when the impactor changes direction) and the initial velocity is measured at the time of collision. In a perfectly elastic impact, where no energy is lost due to "plastic" response of the material, as well as heat, sound, or friction, the coefficient would be 1. However, in real impacts, the coefficient is always lower than 1, indicating that some energy is lost permanently. A lower coefficient means more energy was lost during the impact, which resulted in because of cracking, damage and/or irreversible deformation. The value of the coefficient gives an indication of the permanent damage (energy dissipation) caused by the impact, taking into account the constant energy losses due to heat, sound, and friction. Thus, a quantitative evaluation of the specimens' ability to withstand multiple impacts and recovery can be made based on the rebound height analysis [26,39].

$$Restitution\ coefficient\ (RC) = \frac{v}{u} = \frac{\sqrt{2gh_f}}{\sqrt{2gh_0}} = \sqrt{\frac{h_f}{h_0}} \tag{1}$$

Improved energy dissipation due to self-healing was calculated (Eq. (2)) by dividing the change in restitution coefficient because of healing by the restitution coefficient of the slab at the last impact before healing ($RC_{pre\text{-}healing}$). $RC_{post\text{-}healing}$ is the restitution coefficient from the first impact on the same slab after healing.

$$Improved\ energy\ dissipation = \frac{RC_{pre-healing} - RC_{post-healing}}{RC_{pre-healing}} \tag{2}$$

The deflection of the specimens under impact was determined by analysing the laser data. The laser was directed to the same spot on the specimen before and after healing. The recovery in stiffness was then derived from the moving average deflection value before ($\Delta_{pre\text{-}healing}$) and after healing ($\Delta_{pre\text{-}healing}$), as calculated by Eq. (3). The moving average for 3 data points was utilized for the analysis due to the high scattering of deflection values in the consecutive readings and to avoid over/underestimating the healing capabilities. This measurement was analysed only for the primary impact, not the subsequent rebound impacts.

$$Improved\ stiffness = \frac{\Delta_{pre-healing} - \Delta_{post-healing}}{\Delta_{pre-healing}} \tag{3}$$

### 2.4. Natural frequency analysis

Natural frequency measurements were used to monitor the

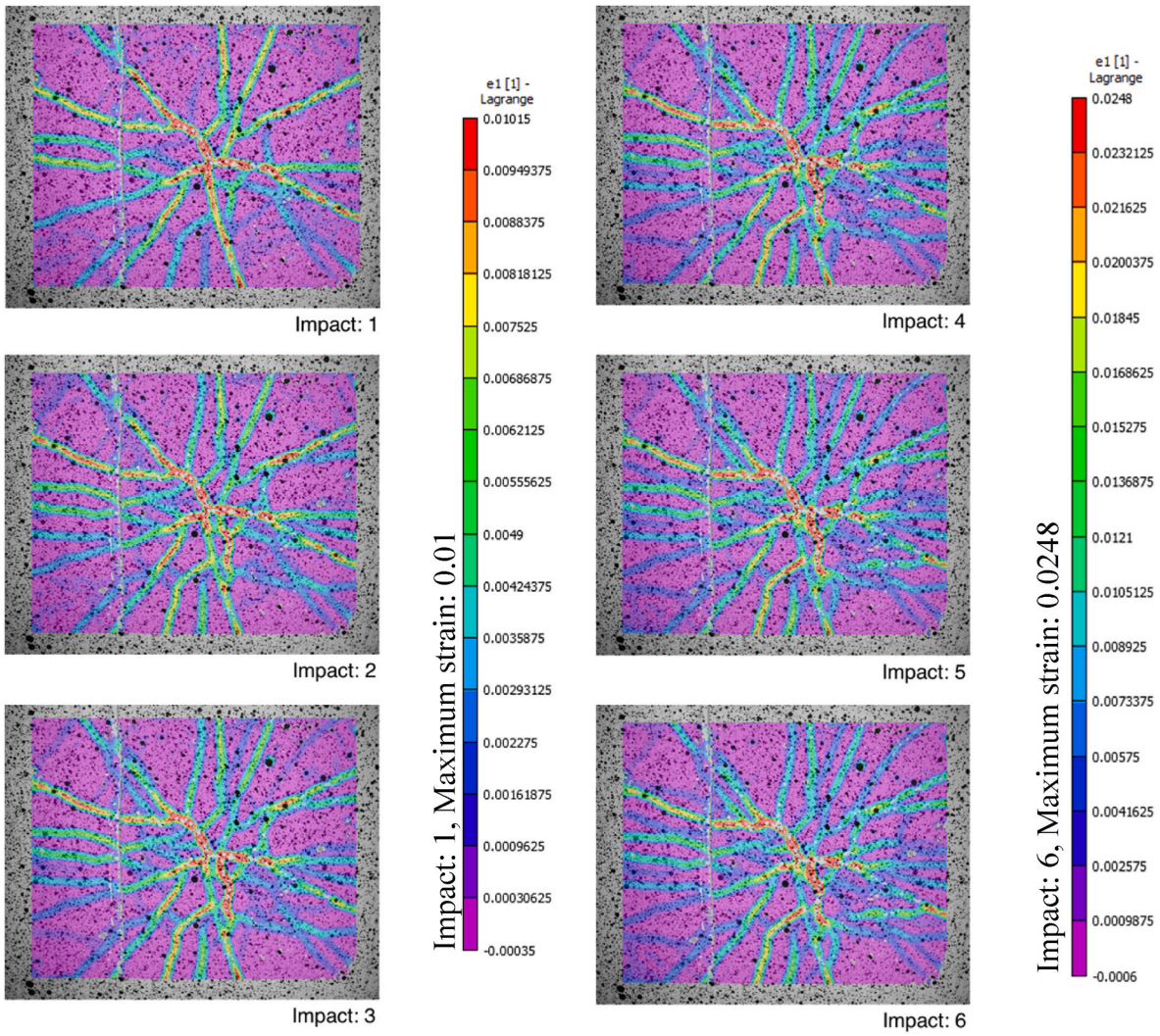


**Fig. 4.** DIC images of the initial impacts showing multiple cracks in the specimen WS5.

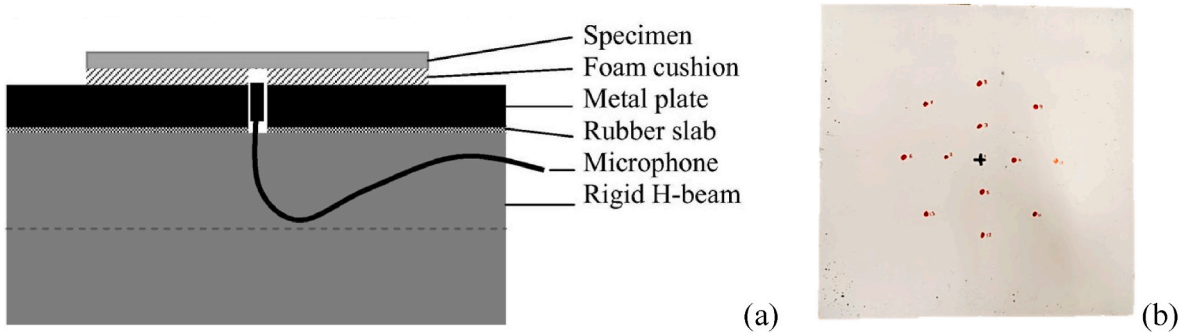


**Fig. 5.** (a) Microphone natural frequency setup as used by Snoeck et al. [26]; (b) thirteen red colour marks indicating where the specimen was tapped by a small hammer.

progression of damage and healing in the tested slabs, as detailed in Snoeck et al. [26]. An illustration of the test setup is shown in Fig. 5. The base structure utilized for the test consisted of a portion of an H-beam and a metal plate with a hole in the middle. A rubber slab was positioned between the beam and metal plate to facilitate good contact between the two components. A foam cushion with a hole in the middle was placed on top of the metal plate, and specimens were positioned on top of this cushion with the impacted side facing downwards during analysis. The foam cushion prevented the specimens from moving around during testing and minimized sound leakage to the surrounding. An upward-directed Sharkoon SN1 microphone was positioned beneath the hole in the foam and the steel plate of the rigid base to capture the acoustic response of the plate when struck with a hammer, with a sampling frequency of 8000 Hz. All specimens were tested in a dry state, as the presence of water within the samples would have elevated the natural frequency of the plates. Therefore, all samples were stored for

24 h under laboratory conditions (20 ± 2 °C and 60% relative humidity) before acoustic analysis, in order to reduce this influence. The tests involved tapping the plates with a small hammer at fixed locations, with measurements taken at 13 points on each plate. The centre of the plate and four points at 3 cm from the centre, and eight points at 7 cm away from the centre were examined. The collected data from the acoustic response were then converted into the frequency domain using the Fast Fourier Transform (FFT) in MATLAB. A peak-picking method was used to collect maximum value of the frequency for all 13 points and then the values were averaged. The test was repeated at intervals of 0, 3, 7 days, and 1, 2, and 4 months on specimens that underwent continuous healing following the impact pre-healing. For the specimens undergoing repeated impact/healing, the test was carried out at the same time intervals as for continuously healing specimens up to the first month, but after each subsequent impact at the first and second months, the intervals were changed to 0, 3, 7, 14 days, and 1 month, with a final test (4 months from the first impact) at the end of the overall healing process.

The natural frequency (NF) was used to calculate the damage and healing indices. The damage index was determined by dividing the decrease in natural frequency caused by the impact by the original frequency before the impact as per Eq. (4). The recovery index was determined by dividing the increase in natural frequency during healing by the decrease in natural frequency caused by the initial impact, as per Eq. (5), $\nu$ being in both equations the natural frequency (Hz).

$$Damage\ index = \frac{\nu_{before\ impact} - \nu_{after\ impact}}{\nu_{before\ impact}} \quad (4)$$

$$Recovery\ index = \frac{\nu_{healing\ stage,t} - \nu_{after\ impact}}{\nu_{before\ impact} - \nu_{after\ impact}} \quad (5)$$

### 2.5. Crack closure quantification

Microscopic images of the cracks were taken at various stages of self-healing: immediately after the initial impact, and after 1, 2, and 4 months of healing. For specimens that were re-impacted after 1 and 2 months, the microscopic images were taken before and after the re-impact. A 3 cm long crack section was chosen on each slab within a distance of 10 cm from the centre, randomly, to observe its closure over time. The images of each crack section were combined using Adobe Photoshop, and the crack area and average width were measured. The UHPC mixture caused the formation of cracks in close proximity to each other, resulting in small cracks (<50 μm) in almost all randomly selected crack sections of the specimens, in addition to the main crack observed (50–150 μm). Some researchers have noted that in the presence of water, crack closure is generally limited to a boundary of 30–50 μm, and beyond 150 μm, the degree of crack closure is anticipated to be minimal [23,30,40,41]. So, in order to gain a better understanding of the autogenous healing for cracks of varying widths, two different ranges of crack sizes were analysed (<50 μm and 50–150 μm) to calculate the index of crack closure as per Eq. (6).

$$Index\ of\ crack\ closure = \frac{A_{crack,0} - A_{crack,t}}{A_{crack,0}} \times 100 \quad (6)$$

Where ($A_{crack,0}$) is the initial crack area after the impact (pre-healing)

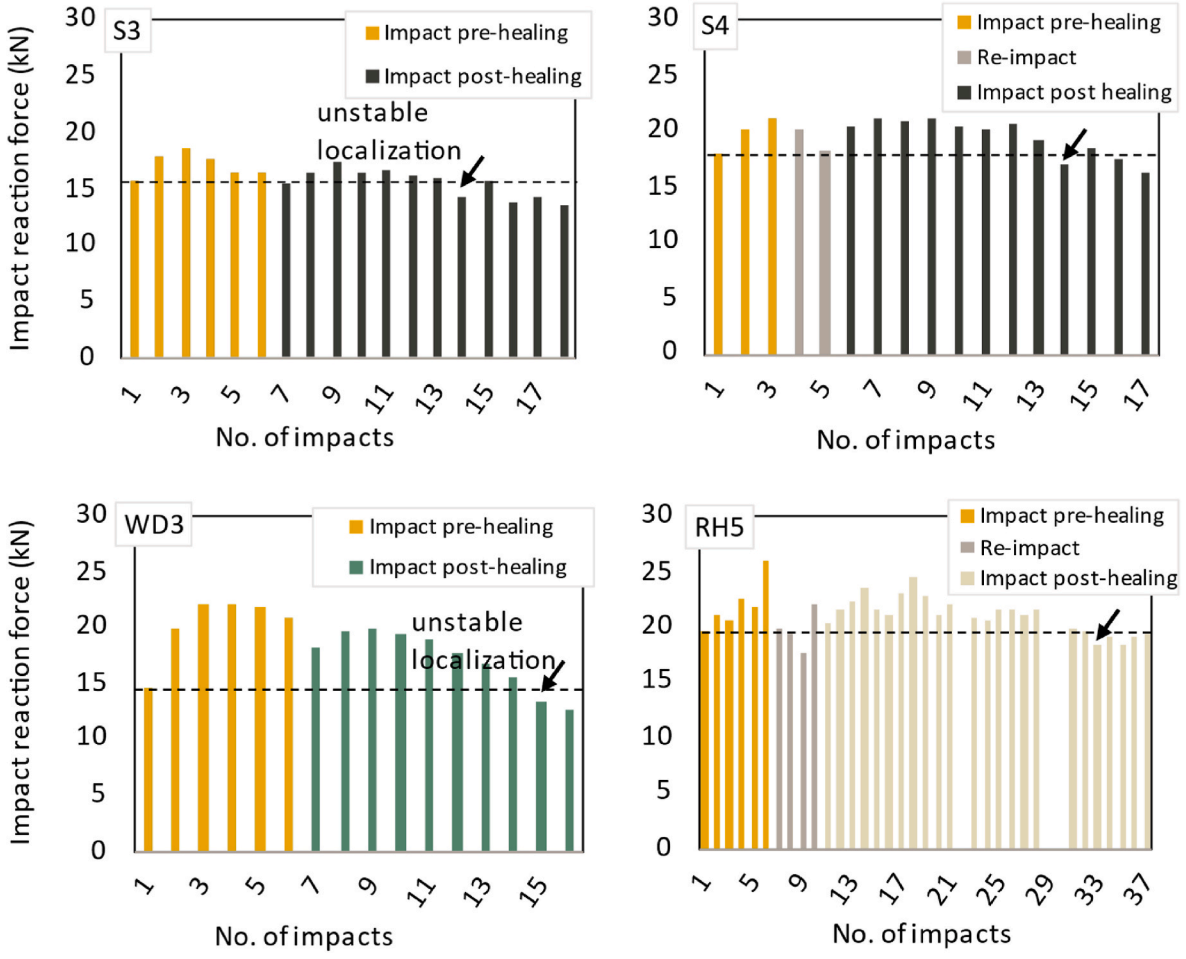


**Fig. 6.** Average impact reaction force from the impact load cells used as an indicator to stop the repeated impact on a specimen based on the subsequent values of the reaction force falling below the first reaction force of pre/post-healing impacts.

and ($A_{crack,t}$) is the area of the crack at time t during the healing period.

## 3. Results and discussion

### 3.1. Load cell measurements

The results of the load cell measurements showed that most specimens displayed strain/deflection-hardening properties, both initially and after the healing period, as shown in Fig. 6 for specimens representative of the three healing conditions. This allowed for the definition of the failure criterion without the specimens being completely perforated or ruptured. After the failure point it was observed that the specimens exhibited either a cone cracking or radial cracking pattern under repeated impacts, as illustrated in Fig. 7. The exact number of repeated impacts on the each slab and the unstable localization point is provided in Table 5. The impact reaction force did not provide a clear trend among the different healing environments. The improvement in impact resistance due to autogenous self-healing was therefore rather quantified using rebound height, laser displacement measurements and natural frequency analysis as discussed in the sub-sections below.

The complete set of results referring to all the tested specimens is collected into the supplementary materials.

### 3.2. Rebound height of the specimens

The impactor velocity becomes zero at the maximum rebound height, capturing it on 120 fps video was possible, as shown in Fig. 8 for frames 11 and 12 the rebound heights were consistent at their maximum. The frame number was counted from the moment the impactor stroke the slab. Rebound heights ranging between 10 and 20 cm were recorded for the 10 kg impactor after a 1 m drop.

From the rebound height, the restitution coefficient was calculated using equation (1) and plotted against the number of impacts, as shown in Fig. 9, to evaluate the energy dissipation capacity of the material before and after healing. Restitution coefficient and energy dissipation of the slab under repeated impacts are inversely proportional. The graph indicates that the restitution coefficient of the reference specimens initially increased for a few impacts up to the dotted line marked on the graph, which was up to 30% increase from the first impact, indicating a decrease in energy dissipation by the specimens upon repeated impacts. The reduction in energy dissipation was attributed to a decrease in the rate of crack formation (as seen in DIC images) and strain-hardening properties. In other words, specimens act more and more like a spring as the number of cracks and depth of the cracks increase, and more fibres start to bridge them, resulting in decreased energy dissipation. The restitution coefficient then remained at the same level with a bit of scattering due to fibre pull-out from the matrix. As cracks deepened and widened, more fibres started to bridge the cracks. Towards the end of the test, there was an increase in the restitution coefficient trend due to strain softening, were unstable localization happens, resulting in decreased energy dissipation. Increase in coefficient of restitution following identical impacts at the same point was also observed by Weir et al. [42] on elasto-plastic materials during low-velocity normal impacts. The material was expected to become more plastic upon repeated impact, but the opposite was observed with an increase in the restitution coefficient (increase in elasticity). This elastic behaviour was due to the majority of the impact loads being governed by the fibres, resulting from an increase in the number of fibres bridging the cracks. Load cell readings also showed strain hardening at the beginning of the test, followed by strain softening, which defined the unstable localization. The test was stopped at this point.

The restitution coefficient was afterwards calculated for the self-healed specimens in different healing environments by impacting the specimen at the same location with the same boundary conditions. As shown in Fig. 10 (only few graphs are represented here; Supplementary Material contains all the graphs), the restitution coefficient of the specimens decreased under the impact load after healing which means energy dissipation of the specimen increased due to self-healing. The increase in energy dissipation was caused by matrix densification [15], the scattering of healing products in the cracks and around the fibre-concrete interface [34] and also due to the formation of new cracks due to the self-healing of previously formed cracks. Fig. 11 displays Digital Image Correlation (DIC) images that highlight distinctions in crack formation pre- and post-healing. After the initial healing, the impact reveals the reopening of localized cracks in regions where the strain was at its maximum before healing. However, non-localized cracks do not reopen to the same extent as before healing. Additionally, the healing process leads to the emergence of new crack formations or high-strain regions which are circled in black. This phenomenon could explain the observed increase in energy dissipation during some repeated impacts following the healing process. The relative difference in energy dissipation before and after healing was analysed by taking the last reading of impact pre-healing and the first reading of impact post-healing. As a matter of fact, there is not any clear pattern among the healed specimens under different environments and different healing periods (Fig. 12). The overall increase in energy dissipation was around 10%.

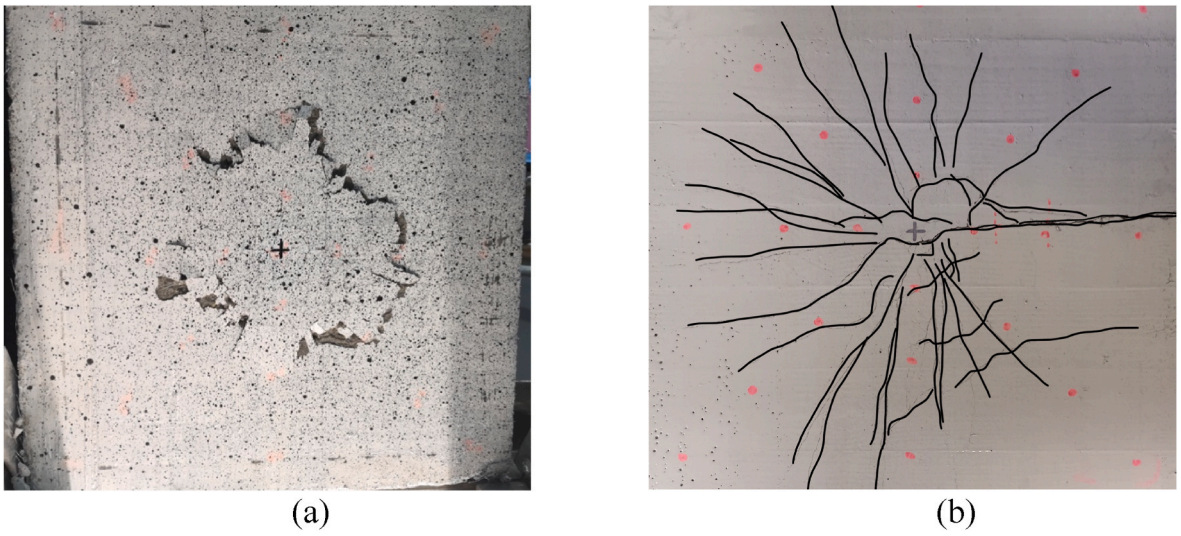


**Fig. 7.** Typical cone cracking (a) and radial cracking (b) patterns were observed under repeated impact loading.

**Table 5**
Number of repeated impacts on the different slabs at each interval.

| Slabs | Specimens | Impacts pre-healing | Re-impact (1 M) | Re-impact (2 M) | Impact post-healing (2 M/4 M) | Total no. of repeated impacts | Unstable localization |
|---|---|---|---|---|---|---|---|
| 1 | S1 | 6 | – | – | >50 | >50 | >50 |
| | WD1 | 6 | – | – | >50 | >50 | >50 |
| | RH1 | 6 | – | – | >50 | >50 | Uncertain trend |
| | REF1 | 51 | – | – | – | 51 | 39 |
| 2 | S2 | 6 | – | – | 6 | 12 | 9 |
| | WD2 | 6 | – | – | 5 | 11 | Uncertain trend |
| | WS2 | 6 | – | – | 14 | 20 | 13 |
| | RH2 | 6 | – | – | 12 | 18 | 16 |
| 3 | S3 | 6 | – | – | 12 | 18 | 13 |
| | WD3 | 6 | – | – | 10 | 16 | 14 |
| | RH3 | 6 | – | – | 23 | 29 | 13 |
| | REF3 | 26 | – | – | – | 26 | 19 |
| 4 | S4 | 3 | 1 | 1 | 12 | 17 | 13 |
| | WD4 | 3 | 1 | 1 | 12 | 17 | Uncertain trend |
| | RH4 | 3 | 1 | 1 | 6 | 11 | 7 |
| | REF4 | 11 | – | – | – | 11 | 8 |
| 5 | S5 | 6 | 2 | 2 | 20 | 30 | 23 |
| | WD5 | 6 | 2 | 2 | 28 | 38 | 32 |
| | WS5 | 6 | – | – | 27 | 33 | Uncertain trend |
| | RH5 | 6 | 2 | 2 | 27 | 37 | 32 |
| 6 | WS6 | 3 | – | – | 17 | 20 | Uncertain trend |

*uncertain trend - For a few specimens, load cell reaction under repeated impacts did not show clear unstable localization.

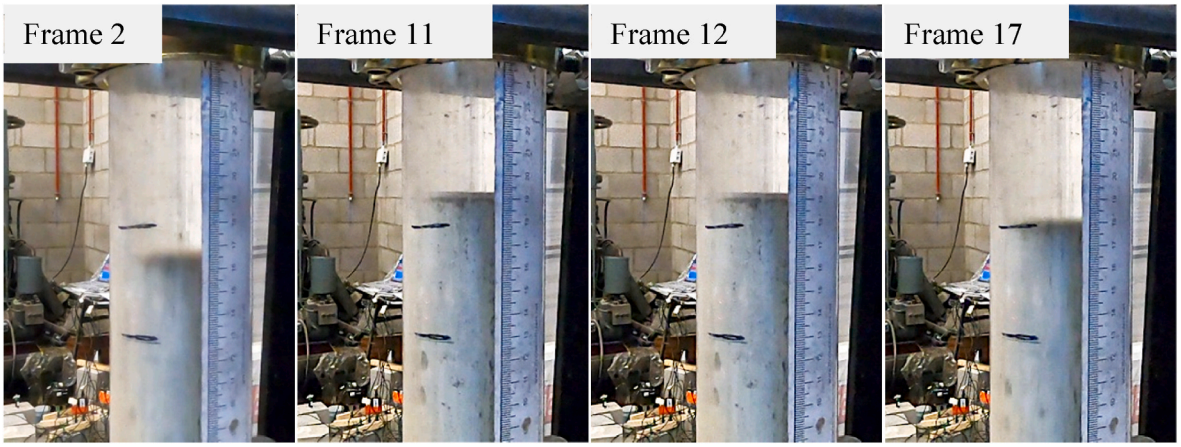


**Fig. 8.** Rebound height of the impactor for different frames captured in a 120-fps video.

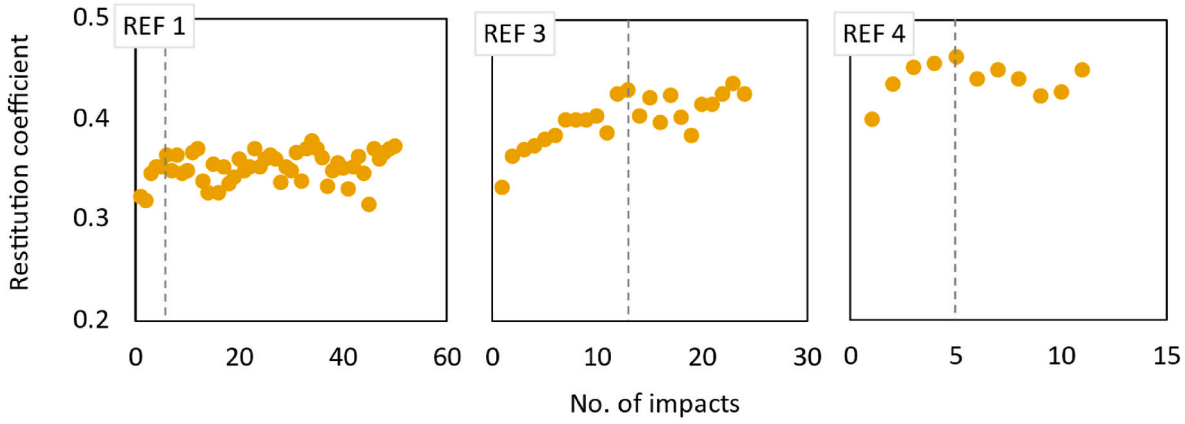


**Fig. 9.** Restitution coefficient of reference specimens under monotonically increasing impacts (initial increase in restitution coefficient is marked with the dotted lines).

### *3.3. Deflection of the specimens under impact*

Fig. 13 shows the deflection of specimens under the impacts for reference specimens without healing. It shows a pattern that the subsequent impacts at the same location increased the deflection. After the first few impacts, the resistance against the impact was mostly governed

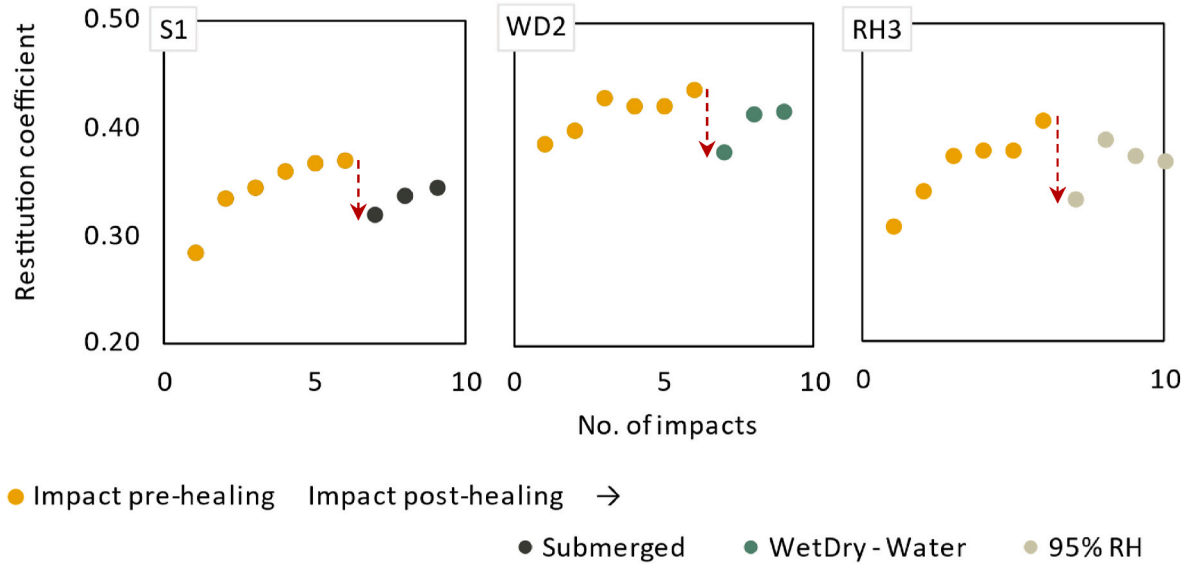


**Fig. 10.** Restitution coefficient of selected autogenously healed specimens under different healing environment.

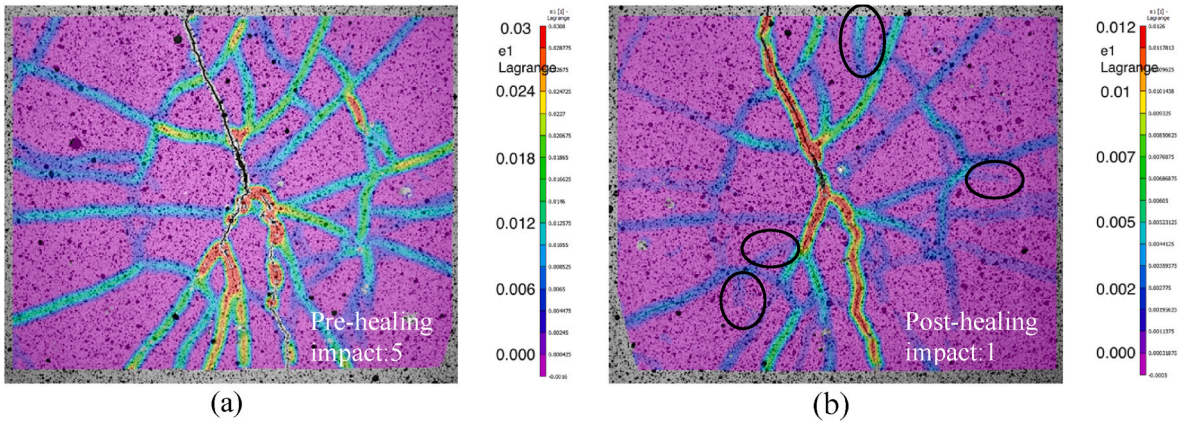


**Fig. 11.** DIC images of a specimen S3 after five repeated impacts before healing (a) and first impact after healing (b). Black circles in the images indicates the formation of a new crack or a high-strain area.

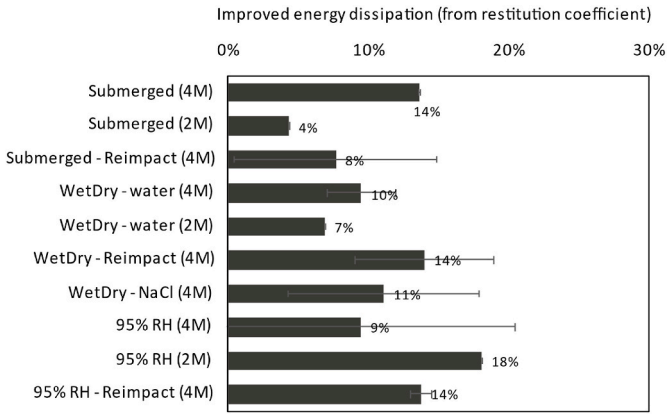


**Fig. 12.** Improved energy dissipation of the specimens after self-healing.

by the fibres, which were slowly pulled out in the subsequent impacts, also seen in DIC images. This was the reason for an increase in the deflection of a specimen under repeated impacts. The deflection was furthermore governed by the failure pattern. Most specimens experienced cone cracking and multiple radial cracks on the tension side, which would increase deflection under repeated impacts. A few specimens showed a deviating failure pattern, where the localized crack ran in the middle of the specimens, cutting them in half, which resulted in diverging boundaries. In this case, the deflection of the specimen did not show an increase in the trend under repeated impact, it showed rather multiple increases and decreases in deflection for REF 3.

After the healing, the specimens were repositioned on the setup exactly as in the initial impact tests and tested for impact resistance until the failure criterion was reached, as assessed through the load cell's reaction force, consistently and accordingly to what explained in subsection 2.3. Fig. 14 shows that the deflection of the specimen was reduced after the healing (for the same impactor dropped from the same height). Upon repeated impacts, the healed specimen showed increasing deflection similar to that of reference specimens. Fibres played a huge role in the latter stage of pre-healing impacts, where strain/deflection hardening was seen in the load cell values. So, the observed reduction in deflection and corresponding increase in stiffness can be likely attributed to the autogenous self-healing happening at the fibre-concrete matrix interface, which strengthened the bond between them. Moreover, the amount of slippage that happened under the impacts was greatly reduced, and that was also reflected in the laser reading. Cuenca et al. and Al-Obaidi et al. demonstrated the regain in fibre/matrix bond

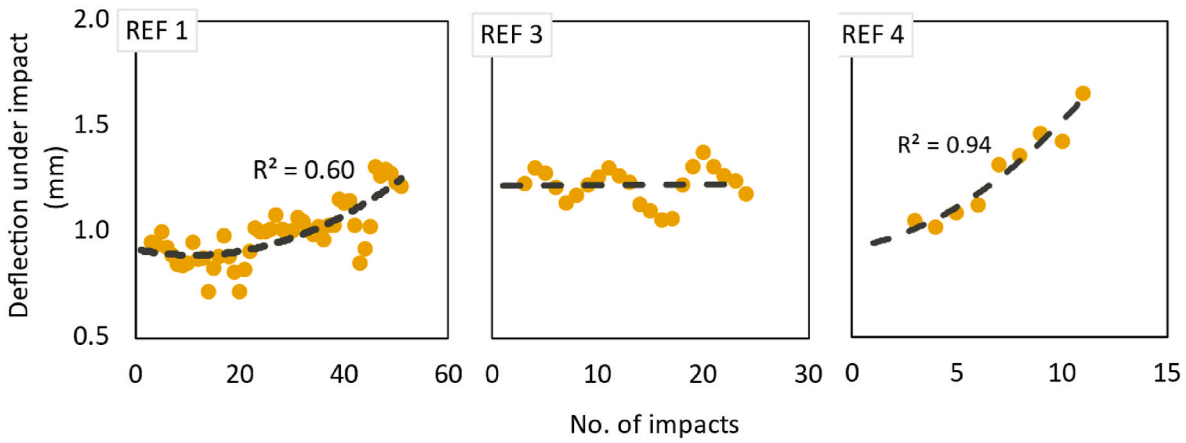


**Fig. 13.** Maximum deflection at the centre of the specimens along the impact trajectory for repeated impacts.

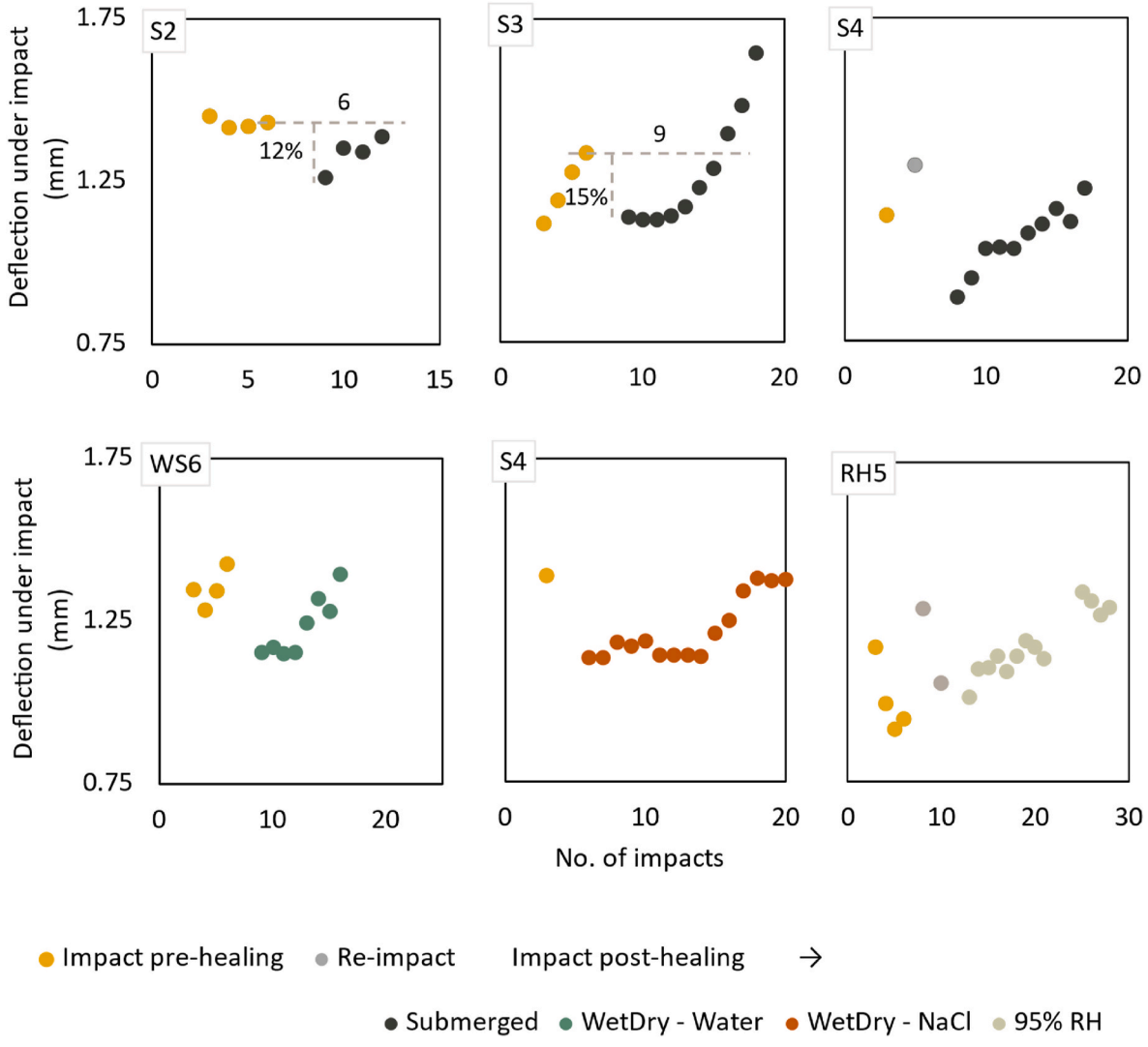


**Fig. 14.** Maximum deflection at the centre of the self-healed specimens under repeated impacts for different environmental conditions (for some representative specimens).

strength due to autogenous self-healing with the micro-structural analysis [15,34]. The stiffness regain was calculated by comparing the specimen's deflection before and after healing as per equation (3). Moreover, improved impact resistance was calculated as the number of repeated impacts required to reach the same deflection as before the healing, i.e. counting the number of impacts required to annihilate the gain in stiffness due to autogenous healing, as shown in Fig. 14 for some representative specimens at least one in each group and remaining

figures are provided in the supplementary materials. The specimens' stiffness and improved impact resistance were calculated and the average for all specimens within each healing environment is plotted in Fig. 15 except for the specimens from slab 1 due to data-saving errors. The difference in deflection between two and four months of healing was not substantial, and results after 2 months were averaged with the ones of four-months in the same healing environment.

Continuously healed specimens showed similar stiffness regain when exposed to the different investigated environmental conditions (submerged, wet/dry-water and 95 ± 5% RH); their improved impact resistance was the same for submerged and wet-dry environments and twice as much as for specimens exposed to 95 ± 5% RH, indicating denser healing around fibres. It was observed that the ones treated with wet/dry-NaCl exhibited greater enhancements in both stiffness and impact resistance compared to other environmental conditions. This could be attributed to the chloride binding capacity of the matrix, which resulted in the formation of additional precipitates in and around the cracks and the interface between the fibres and concrete [14]. In terms of repeated impact/healing scenarios, improved stiffness was in the order of submerged, wet-dry in water, and 95 ± 5% RH, showing that water availability played a crucial role in stiffness gain. For improving the impact resistance for re-impact specimens, the condition of 95 ± 5% RH did not lead to much gain due to repeated damage. While submerged and wet-dry conditions induced significant stiffness improvement but could not lead to a clear conclusion about which healing environment results in improved impact resistance because the test was stopped at the defined failure point (unsteady localization) based on load cell values.

### 3.4. Natural frequency analysis

The natural frequency test was used to monitor the healing progress of the material as it regains its stiffness through autogenous self-healing. Fig. 16a shows the reduction of natural frequency after the initial impacts and its increase with the healing period under different environmental conditions. The uncracked specimens average natural frequency was in the range of 2000–2250 Hz. The measurements were taken at 13 locations on each specimen at various stages of impact and healing. All the natural frequency values were averaged per specimen, and their standard deviation was less than 1%. Furthermore, the data referring to specimens healed under the same conditions were averaged to show the healing trend, and their standard deviation was around 10%–15%, and this significant amount of standard deviation was due to variation in thickness of specimens. As was seen for the deflection, two and four months healed specimens' recovery index was similar.

Fig. 16b illustrates the damage index of all the specimens resulting from the impacts before healing. An average damage index across all the specimens (which were then allocated to the different healing environments) was 29 ± 2%. The specimens from the same slab showed similar damage indexes, and they were evenly distributed among the different healing conditions to eliminate the influence of the slab on the results obtained for one particular healing environment. This approach ensured that any differences in geometry would not interfere with the analysis of the recovery index. Fig. 16c shows after three days of healing, the submerged specimens and those in wet-dry cycles with NaCl showed a 70% recovery ratio, while the wet-dry specimens in water featured a 60% recovery. The specimens in 95 ± 5% relative humidity showed the lowest recovery ratio of 40%. After four months of healing, the submerged specimens had fully recovered 90% of their initial frequency, the specimens experiencing wet-dry cycles recovered between 80 and 90%, no matter the salinity of the water, and the specimens in 95 ± 5% relative humidity showed 65% recovery. The specimens' healing capability improved with the healing period duration, and the recovery rate was linked to water availability. The increase in natural frequency was caused by the hydration of unhydrated cement particles in the concrete matrix, which resulted from the low water-cement ratio in the original mix and the limited space for complete hydration. Therefore, the majority of the increase in natural frequency occurred in the first three days, as after crack formation, the $Ca^{2+}$ ions diffused towards the crack surfaces from the inner concrete matrix containing rich calcium ions and formed new calcium silicate hydrates and $CaCO_3$ precipitation on the crack surfaces leading to closing of the narrow cracks in a short period of time. Over time, wider cracks also partially closed, leading to a further increase in natural frequency [27,43,44].

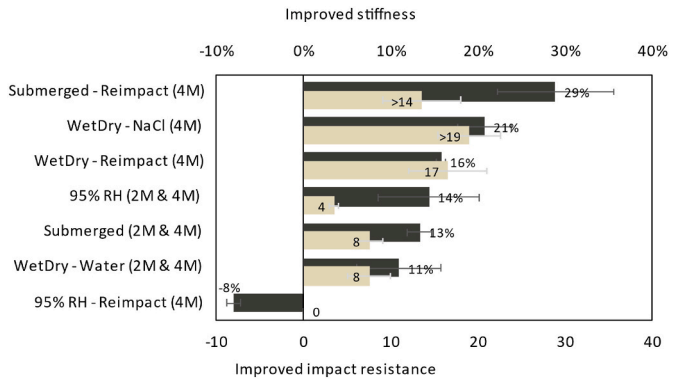


**Fig. 15.** Stiffness gain (black) and improved impact resistance (grey) of specimens under different healing environments. The difference in deflection between two and four months of healing was not substantial, and results after 2 months were averaged with the ones of four-months specimens in the same healing environment.

For the repeated impact/healing scenario, as depicted in Fig. 17, the specimens were subjected to repeated impacts at the end of the first and second month of healing, resulting in dropping in natural frequency, as indicated by the red arrows pointing downwards. The green arrow represents the recovery of the material over time, which was observed both after the initial impact and upon repetition of the impact/healing cycles. This material shows the ability to heal multiple times after repeated impacts. However, the healing performance of the specimens in the high relative humidity environment was found to be lower after the second re-impact, with a recovery index of less than 30% as compared to previous healing cycles. Meanwhile, the specimens stored in submerged and wet-dry conditions showed their higher resilience in repeated impact/healing. A similar behaviour of the repeated impact/healing of a concrete matrix by using natural frequency was demonstrated by Snoeck et al. [26].

A clear comparison between the recovery index for continuous healing and repeated impact/healing can be seen in Fig. 18. At the end of four months, the regain in natural frequency under repeated impact/healing is only 10% lower compared to the continuous healing for submerged and wet-dry conditions, while for 95 ± 5% RH it was 30% lower. The decreased recovery observed in the last stage of repeated impact/healing for specimens under high relative humidity could be attributed to the depletion of healing materials near the crack surfaces, which were utilized in previous healing cycles. Additionally, the impermeable nature of UHPC and limited water availability make it difficult for the ions to diffuse from the matrix towards the crack surface, at deeper locations within the crack. However, in the submerged and wet/dry conditions, there was enough water to facilitate the diffusion of ions from further away towards the crack surface, and in time, the regain in natural frequency would be similar to that of continuously healed specimens. The water dependent healing rate was also noticed in the crack closure quantification, as is discussed in the next sub-section 3.5.

### 3.5. Crack closure quantification

Microscopic images were captured at various stages of the healing process, including after the initial impacts and at 1, 2, and 4 months for continuous healing, and additionally after re-impact at 1 and 2 months

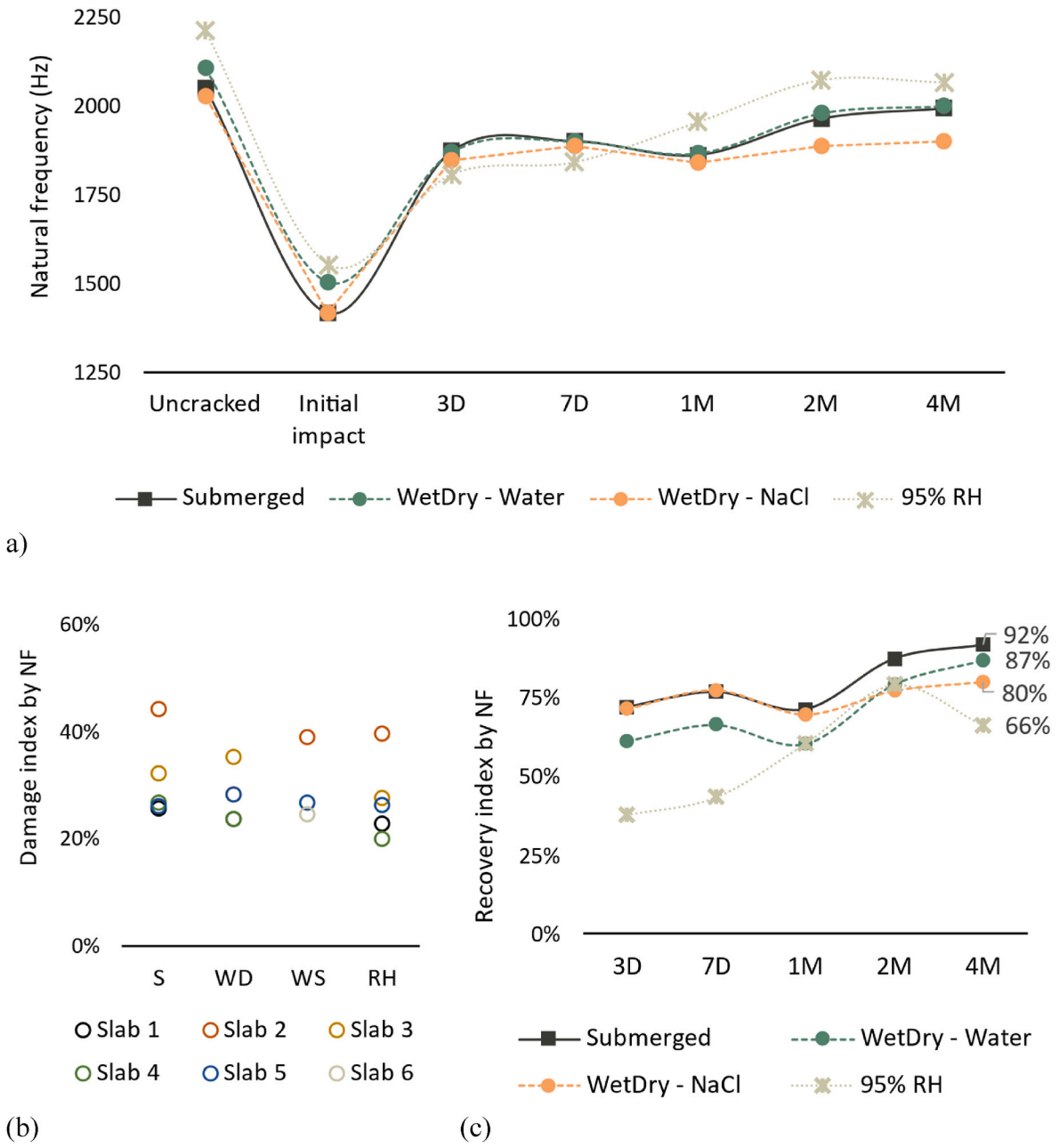


**Fig. 16.** Natural frequencies of the continuously healed specimens when being exposed to different healing environments (a), their damage index (b), and recovery index (c).

for repeated impact/healing. The cracks have been divided into two categories based on their width, less than 50 μm and between 50 and 150 μm, to study the influence of crack width on healing in different environments, as shown in Fig. 19. For continuously healed specimens, after the first month of healing, the crack closure rate for the submerged specimens was 89% for cracks less than 50 μm, 43% for wet/dry in water, 57% for wet/dry in NaCl, and 16% for 95 ± 5% RH. For cracks between 50 and 150 μm, the closure rate was 78% for submerged specimens, 14% for wet/dry in water and NaCl, and no significant closure was observed for 95 ± 5% RH. This indicates that small cracks heal faster in all environments with higher water availability, even in the form of moisture. After four months of healing, the submerged specimen's cracks were completely healed for both width categories. The closure rate for wet/dry was between 70 and 100%, and for 95 ± 5% RH, between 20% and 40%, with larger closure for cracks narrower than 50 μm and lower closure for cracks between 50 and 150 μm wide. The cracks clearly show a progressive healing process with time; larger cracks require more time to heal. The primary mechanisms underlying autogenous healing involve the additional hydration of unhydrated particles and the deposition of CaCO3 on the crack surfaces [15,18,20,44].

Fig. 20 represents the evolution of crack closure for the specimens which experienced repetitions of healing and impact stages. The specimens were re-impacted after the first and second months of healing, and the residual crack closure after the re-impact is marked on the chart. The decrease in the crack closure index indicates that the crack either widened or healed materials spalled under the impact. For cracks narrower than 50 μm, at the end of 4 months, the healing performance of the submerged was similar to that of continuously healed specimens, while for specimens in wet/dry conditions, it was 13% lower. However, it could be argued that with more time, specimens would have completely healed. The healing performance at 95 ± 5% RH was

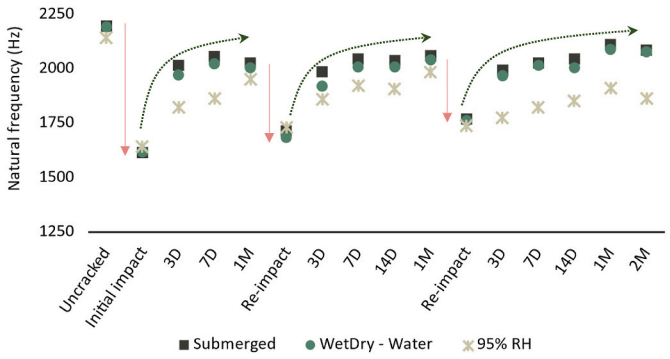


**Fig. 17.** Evolution of natural frequency of the specimens under different healing environment for the repeated impact/healing criteria. A red line pointing downward shows a decrease in natural frequency after impact and an upward green line shows the healing trend.

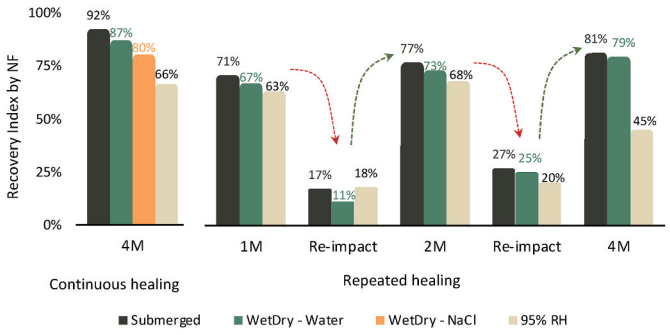


**Fig. 18.** Evolution of recovery index by natural frequency for different healing environments and healing types (continuous healing and repeated impact/healing).

insignificant in the first month of healing. After the first re-impact, the crack widened by 40%, but it narrowed back to its original width by the end of the four months of healing, even after the crack widened again in the second re-impact. The repeated autogenous healing mechanism involves two distinct stages: during the first healing cycles, the crystallization of CaCO3 is primarily surface controlled [15,18,20], while during the subsequent healing cycles, it becomes diffusion controlled. This change is attributed to the diffusion of Ca2+ ions near the crack faces. As a consequence, in later healing cycles, additional Ca2+ ions must diffuse deeper into the matrix before participating in the crystallization process [44].

For cracks between 50 and 150 μm, the total crack closure at the end of four months for submerged and wet/dry was decreased by 30–40% compared to continuously healed specimens. As expectable, larger cracks tend to close more slowly with repeated damage than cracks narrower than 50 μm and the effect of repeated impact on them might be stronger. Cracks in specimens exposed to 95 ± 5% RH were closed slightly after the first re-impact, however, there was no sign of crack closure after the second re-impact. Similarly, in the natural frequency test after the second re-impact, the 95 ± 5% RH recovery index showed a reduced recovery rate compared to the previous healing cycles. This could be due to the fact that under the impact loading larger cracks tend to widen more because those cracks are more likely turning into the "weakest section" in the structural elements as compared to the small cracks. Also, with lower water content and availability the diffusion of the hydrates along the crack surfaces was limited. The aforesaid statements described on the basis of the crack closure index are confirmed and supported by microscopic images of crack closure under different environmental conditions shown in Fig. 21. After four months, the microscopic image of the specimen in wet/dry condition in NaCl solution showed mild corrosion. However, despite this, the material's mechanical performance did not experience significant degradation, as seen in restitution coefficient and stiffness at the end of the four-month period. Furthermore, Davolio et al. [35] conducted a study on the same material to test its self-healing abilities under sustained loading for twelve months across three exposure classes: tap water, NaCl solution, and geothermal water. They discovered that the corrosion only affected the surface of the specimens and did not penetrate the matrix. Therefore, it is reasonable to conclude that the specimen exposed to NaCl did not experience any deterioration from corrosion during the four months period.

## 4. Conclusions

This paper introduces a comprehensive test methodology and validation process aimed at measuring the enhanced impact resistance of Ultra High-Performance Concrete (UHPC) slabs. The improvements are attributed to the stimulated autogenous self-healing effects, resulting in enhanced energy dissipation, stiffness, and natural frequency after the healing period in various healing environments. Continuous and

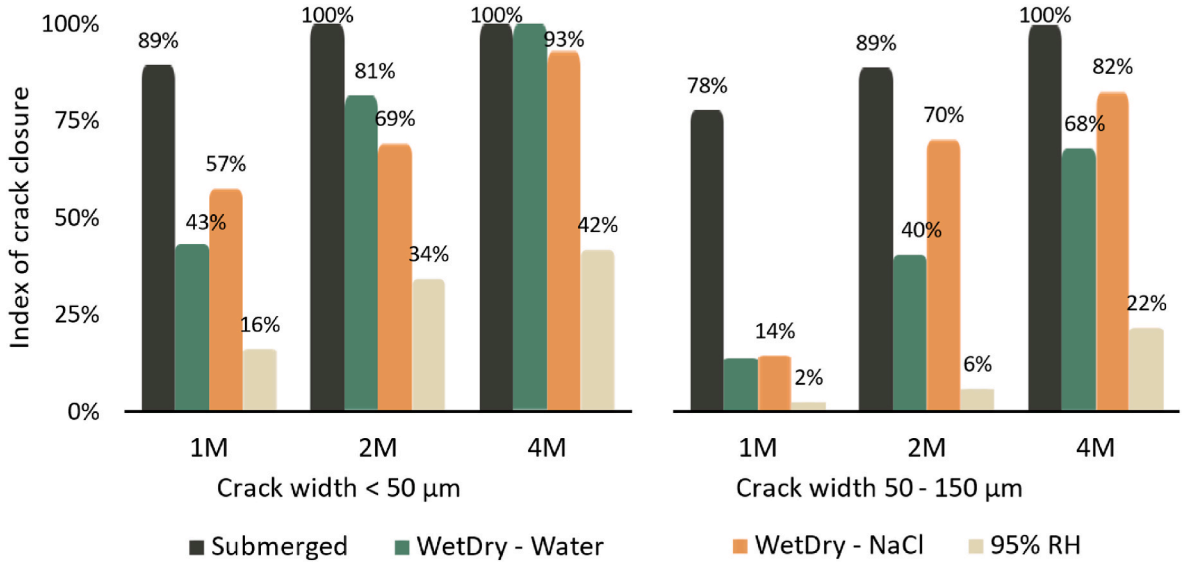


**Fig. 19.** Index of crack closure for the continuously healed specimens under different healing conditions for the crack widths <50 μm and 50–100 μm.

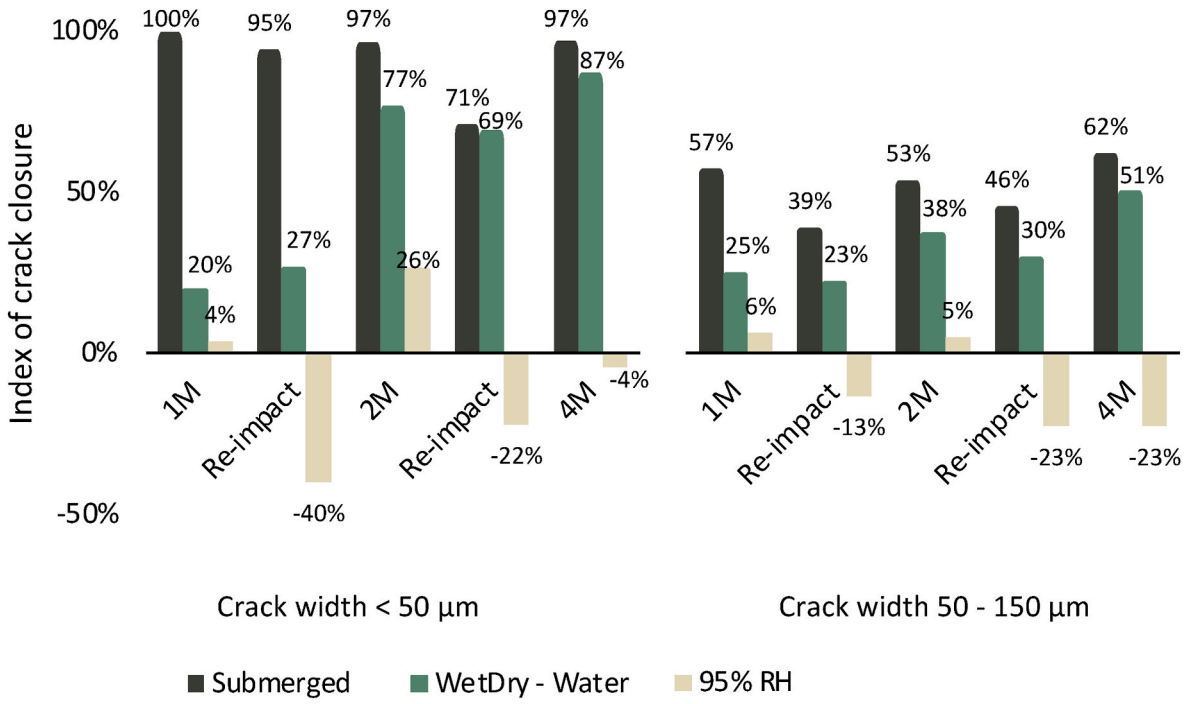


**Fig. 20.** Index of crack closure for repeatedly healed specimens under different healing conditions for the crack widths <50 µm and 50–100 µm.

repeated healing phenomena were clearly distinguished through natural frequency, crack closure quantification, and a subtle variation in material stiffness. Additionally, the study briefly explores the strain-hardening property of UHPC when subjected to repeated impacts and utilizes this information to define the failure point, which is a novel and crucial aspect of the experimental campaign. The quantification of the evolution of surface crack closure, can be related to an increased overall durability of the material against aggressive environments. Based on the findings, several conclusions can be drawn.

- Due to UHPC strain-hardening characteristics, the material has the ability to develop multiple radial cracks when subjected to repeated impacts, which results in increased energy dissipation. Once the healing period is complete, the material can partially or fully recover its energy dissipation capacity.
- After undergoing the healing process, the slab's stiffness increases by up to 30%, and it takes several impacts to return it to its original value (after pre-damage at the starting of the healing period). The stiffness improvement in specimens that underwent continuous healing in different environments was similar, but stiffness dissipated more quickly in specimens healed at 95% relative humidity. The increase in stiffness in repeatedly healed specimens was found to be proportional to the water availability, with the highest regain observed in the specimens submerged in water and the least increase observed in those exposed to 95 ± 5% RH.
- For continuously healed specimens, the natural frequency of the material was restored in the following order for the investigated environmental exposure conditions: submersion in water > wet-dry cycles in water and NaCl >95% RH. Submerged specimens regained over 90% of their natural frequency within four months, while those subjected to wet-dry regained 80–90%, and those exposed to 95 ± 5% RH regained only 65%. In the case of specimens subjected to repeated impact/healing, both submersion in water and exposure to wet-dry cycles induced a regain as high as up to 80% in terms of natural frequency at the end of the assessed 4 months, while the specimens exposed to 95 ± 5% RH regained only about 45%. The low regain in the case of 95 ± 5% RH was attributed to the reduced diffusion of $Ca^{2+}$ ions to the unhydrated binder particles at the crack surface and the lower water availability for hydration.
- In continuously healed specimens over a four-month period, the index of crack closure for crack widths of 50–150 µm was found to be highest in the immersed condition (100% sealed), followed by exposure to wet-dry cycles (70–80% sealed), and lowest in exposure to 95 ± 5% RH (20% sealed). For specimens experiencing repeated impact/healing, the crack closure index reached 60% for the immersed condition and 50% for wet-dry cycles at the end of four months. However, in 95 ± 5% RH specimens, the crack width widened during repeated impacts and did not show any significant crack closure at the end of four months. Specifically, there was not any healing after the repeated impacts at the second interval. This was due to the depletion of available unhydrated cement in the vicinity of the crack surface during the repeated damage. In addition, diffusion rate of $Ca^{2+}$ ions and water towards the unhydrated particles at the crack surface was very low in case of 95 ± 5% RH. The trend of index of crack closure matches with the healing index from the natural frequency test.

In conclusion, the paper's demonstration of Ultra-High-Performance Concrete's (UHPC) autogenous self-healing property has the potential to revolutionize the construction industry, significantly improving impact resistance and durability. As a result, safer, more resilient, and sustainable infrastructure can be developed, capable of withstanding diverse environmental and operational challenges.

## 5. Limitations and future directions

The experimental approach employed in this study was tailored to capitalize on the strain-hardening characteristic of UHPC under repeated impacts, enabling the measurement of energy dissipation, stiffness, and natural frequency. Additionally, the study assessed these parameters after self-healing to showcase the improved impact resistance. However, it should be noted that when subjected to repeated or single impacts beyond the strain-hardening capacity, significant crack opening may occur due to localized crack propagation, and any crack wider than 0.3 mm tends to remain open even after the considerable

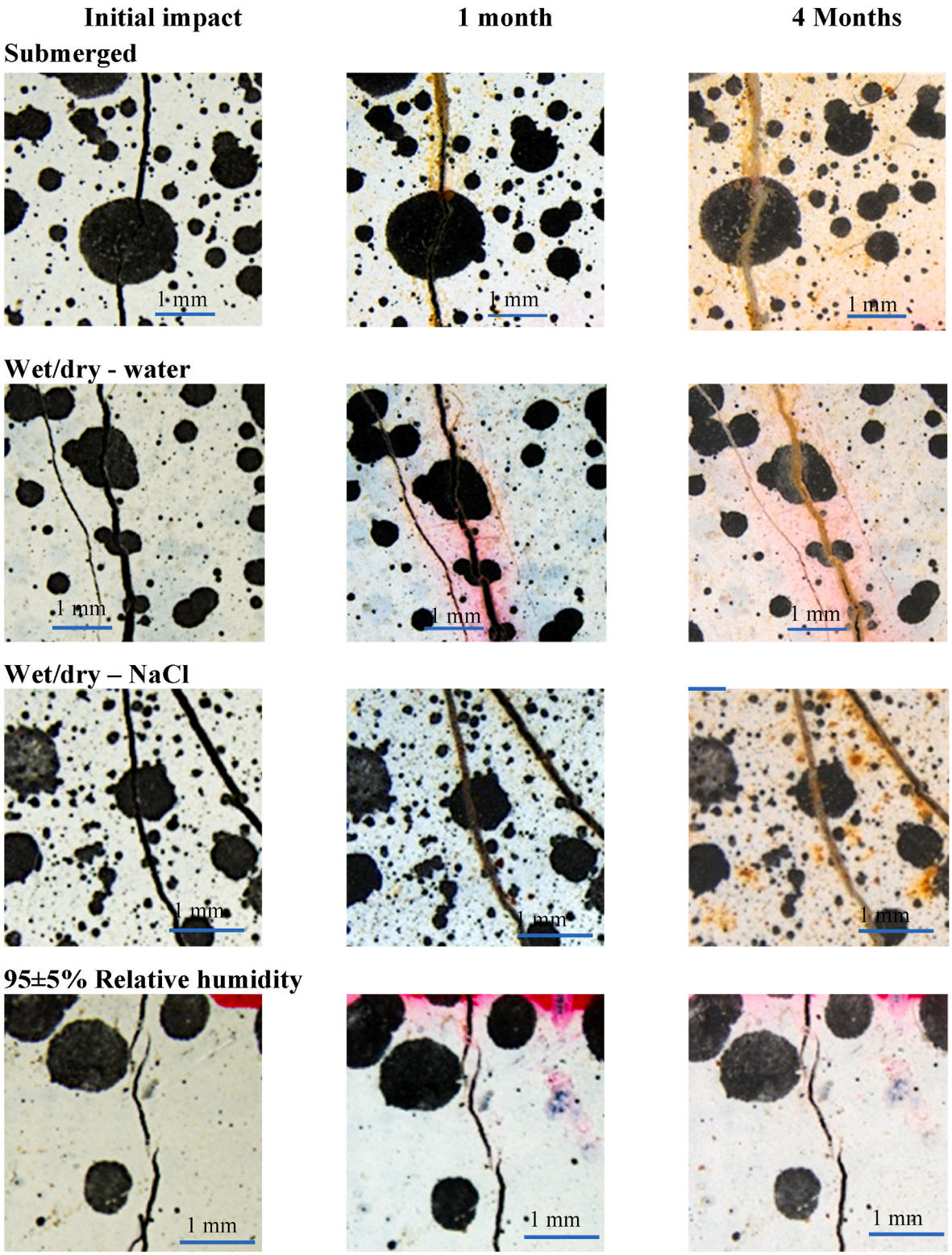


**Fig. 21.** Microscopic images of evolution of crack closure for continuously healed specimens under different healing conditions.

healing period. This reveals a limitation of the autogenous self-healing process. While the impact resistance does improve for cracks wider than 0.3 mm through self-healing, primarily due to the increase in density of the matrix, it fails to enhance long-term durability because of unclosed cracks leading to a gradual reduction in mechanical properties over time. Therefore, it becomes crucial to address both mechanical strength and durability for sustainable improvements, and this experimental campaign is predominantly limited to cracks smaller than 0.3 mm. Additionally, another limitation lies in the applicability of the experimental methodology, mainly to strain-hardening UHPC and Engineered Cementitious Composites (ECC).

In the future, modifications to the experimental methodology could be explored to investigate enhanced impact resistance for crack widths exceeding 0.3 mm, particularly in the context of autonomous self-

healing technologies that utilize micro- and macro-encapsulation and vascular networks.

## Declaration of competing interest

The authors declare that they have no known competing financial interests or personal relationships that could have appeared to influence the work reported in this paper.

## Data availability

Data will be made available on request.

## Acknowledgements

The authors would like to acknowledge the contributions of several individuals who assisted with the lab testing for this study. Specifically, we are grateful to Dr. Roman Wan-Wendner and Mr. Muhammad Arslan Yaqub for their invaluable guidance with the Digital image correlation work. This project has received funding from the European Union's Horizon 2020 research and innovation programme under the Marie Skłodowska-Curie grant agreement No 860006.

## Appendix A. Supplementary data

Supplementary data to this article can be found online at https://doi.org/10.1016/j.cemconcomp.2023.105239.

## References

[1] A.E. Naaman, H.W. Reinhardt, Proposed classification of HPFRC composites based on their tensile response, Mater. Struct. Constr. 39 (2006) 547–555, https://doi.org/10.1617/S11527-006-9103-2/METRICS.

[2] N.P. Kannikachalam, E.C. Asensio, E.M.G. Brac, R. Rosignoli, N. De Belie, L. Ferrara, An experimental methodology to assess effects of healing on freeze-thaw damaged ultra high-performance concrete, in: 6th Fib Int. Congr. Concr. Innov. Sustain., Fib, The International Federation for Structural Concrete, 2022, pp. 280–287.

[3] N.P. Kannikachalam, D.A. Clerque Vela, Y.G. Ocampo Pacheco, F. Lo Monte, N. de Belie, L. Ferrara, Fatigue behavior and effect of stimulated autogenous self-healing in Ultra High-Performance Concrete, in: M. di Prisco, G.B.A. Meda (Eds.), 14th Fib PhD Symp. Civ. Eng., Fib PhD Symposium, Rome, 2022, pp. 297–304, 10.2/JQUERY.MIN.JS.

[4] V. Bindiganavile, N. Banthia, Polymer and steel fiber-reinforced cementitious composites under impact loading - Part 1: bond-slip response, ACI Mater. J. 98 (2001) 10–16, https://doi.org/10.14359/10155.

[5] V. Bindiganavile, N. Banthia, Polymer and steel fiber-reinforced cementitious composites under impact loading - Part 2: flexural toughness, ACI Mater. J. 98 (2001) 17–24, https://doi.org/10.14359/10156.

[6] V. Bindiganavile, N. Banthia, B. Aarup, Impact response of ultra-high-strength fiber-reinforced cement composite, Materials J. 99 (2002) 543–548, https://doi.org/10.14359/12363.

[7] D.Y. Yoo, N. Banthia, Impact resistance of fiber-reinforced concrete – a review, Cem. Concr. Compos. 104 (2019), 103389, https://doi.org/10.1016/J.CEMCONCOMP.2019.103389.

[8] J. Kheir, A. Klausen, T.A. Hammer, L. De Meyst, B. Hilloulin, K. Van Tittelboom, A. Loukili, N. De Belie, Early age autogenous shrinkage cracking risk of an ultra-high performance concrete (UHPC) wall: modelling and experimental results, Eng. Fract. Mech. 257 (2021), 108024, https://doi.org/10.1016/J.ENGFRACMECH.2021.108024.

[9] J. Li, Z. Wu, C. Shi, Q. Yuan, Z. Zhang, Durability of ultra-high performance concrete – a review, Construct. Build. Mater. 255 (2020), 119296, https://doi.org/10.1016/J.CONBUILDMAT.2020.119296.

[10] R.K. Dhir, M.R. Jones, Water permeability and autogenous healing of cracks in concrete, 1999, p. 654, https://doi.org/10.1680/IICSDAC.28241.0047.

[11] D. Snoeck, J. Dewanckele, V. Cnudde, N. De Belie, X-ray computed microtomography to study autogenous healing of cementitious materials promoted by superabsorbent polymers, Cem. Concr. Compos. 65 (2016) 83–93, https://doi.org/10.1016/J.CEMCONCOMP.2015.10.016.

[12] Y. Zhang, R. Wang, Z. Ding, Influence of crystalline admixtures and their synergetic combinations with other constituents on autonomous healing in cracked concrete—a review, Materials 15 (2022), https://doi.org/10.3390/MA15020440.

[13] B. Park, Y.C. Choi, Effect of healing products on the self-healing performance of cementitious materials with crystalline admixtures, Construct. Build. Mater. 270 (2021), 121389, https://doi.org/10.1016/J.CONBUILDMAT.2020.121389.

[14] E. Cuenca, F. Lo Monte, M. Moro, A. Schiona, L. Ferrara, Effects of autogenous and stimulated self-healing on durability and mechanical performance of UHPFRC: validation of tailored test method through multi-performance healing-induced recovery indices, Sustain. Times 13 (2021), 11386, https://doi.org/10.3390/SU132011386, 13 (2021) 11386.

[15] E. Cuenca, A. Mezzena, L. Ferrara, Synergy between crystalline admixtures and nano-constituents in enhancing autogenous healing capacity of cementitious composites under cracking and healing cycles in aggressive waters, Construct. Build. Mater. 266 (2021), 121447, https://doi.org/10.1016/j.conbuildmat.2020.121447.

[16] N.P. Kannikachalam, D. di Summa, R.P. Borg, E. Cuenca Asensio, M. Parpanesi, N. De Belie, L. Ferrara, Assessment of sustainability and self-healing performances of recycled ultra-high-performance concrete, ACI Mater. J. 120 (2023) 117–132, https://doi.org/10.14359/51737336.

[17] F. Lo Monte, L. Ferrara, Self-healing characterization of UHPFRCC with crystalline admixture: experimental assessment via multi-test/multi-parameter approach, Construct. Build. Mater. 283 (2021), 122579, https://doi.org/10.1016/J.CONBUILDMAT.2021.122579.

[18] E. Cuenca, L. D'Ambrosio, D. Lizunov, A. Tretjakov, O. Volobujeva, L. Ferrara, Mechanical properties and self-healing capacity of ultra high performance fibre reinforced concrete with alumina nano-fibres: tailoring ultra high durability concrete for aggressive exposure scenarios, Cem. Concr. Compos. 118 (2021), 103956, https://doi.org/10.1016/j.cemconcomp.2021.103956.

[19] E. Cuenca, M. Criado, Mercedes Giménez, C. Alonso María, L. Ferrara, Effects of Alumina Nanofibers and Cellulose Nanocrystals on Durability and Self-Healing Capacity of Ultrahigh-Performance Fiber-Reinforced Concretes, J. Mater. Civ. Eng. 34 (2022), 04,022,154, https://doi.org/10.1061/(ASCE)MT.1943-5533.0004375.

[20] E. Cuenca, V. Postolachi, L. Ferrara, Cellulose nanofibers to improve the mechanical and durability performance of self-healing Ultra-High Performance Concretes exposed to aggressive waters, Construct. Build. Mater. 374 (2023), 130785, https://doi.org/10.1016/J.CONBUILDMAT.2023.130785.

[21] B. Xi, S. Al-Obaidi, L. Ferrara, Effect of different environments on the self-healing performance of Ultra High-Performance Concrete – a systematic literature review, Constr. Build. Mater. 374 (2023) 130946. https://doi.org/10.1016/J.CONBUILDMAT.2023.130946.

[22] B. XI, Z. Huang, S. Al-Obaidi, L. Ferrara, Predicting High-Performance Concrete (UHPC) self-healing performance using hybrid models based on metaheuristic optimization techniques, Constr. Build. Mater. 381 (2023) 131261. https://doi.org/10.1016/J.CONBUILDMAT.2023.131261.

[23] Y. Yang, M.D. Lepech, E.H. Yang, V.C. Li, Autogenous healing of engineered cementitious composites under wet-dry cycles, Cement Concr. Res. 39 (2009) 382–390.

[24] D. Homma, H. Mihashi, T. Nishiwaki, Self-healing capability of fibre reinforced cementitious composites, J. Adv. Concr. Technol. 7 (2009) 217–228.

[25] H. Ma, S. Qian, Z. Zhang, Effect of self-healing on water permeability and mechanical property of Medium-Early-Strength Engineered Cementitious Composites, Construct. Build. Mater. 68 (2014) 92–101, https://doi.org/10.1016/J.CONBUILDMAT.2014.05.065.

[26] D. Snoeck, T. De Schryver, N. De Belie, Enhanced impact energy absorption in self-healing strain-hardening cementitious materials with superabsorbent polymers, Construct. Build. Mater. 191 (2018) 13–22, https://doi.org/10.1016/J.CONBUILDMAT.2018.10.015.

[27] N. De Belie, E. Gruyaert, A. Al-Tabbaa, P. Antonaci, C. Baera, D. Bajare, A. Darquennes, R. Davies, L. Ferrara, T. Jefferson, C. Litina, B. Miljevic, A. Otlewska, J. Ranogajec, M. Roig-Flores, K. Paine, P. Lukowski, P. Serna, J. M. Tulliani, S. Vucetic, J. Wang, H.M. Jonkers, A review of self-healing concrete for damage management of structures, Adv. Mater. Interfac. 5 (2018) 1–28, https://doi.org/10.1002/admi.201800074.

[28] L. Ferrara, T. Van Mullem, M.C. Alonso, P. Antonaci, R.P. Borg, E. Cuenca, A. Jefferson, P.L. Ng, A. Peled, M. Roig-Flores, M. Sanchez, C. Schroefl, P. Serna, D. Snoeck, J.M. Tulliani, N. De Belie, Experimental characterization of the self-healing capacity of cement based materials and its effects on the material performance: a state of the art report by COST Action SARCOS WG2, Construct. Build. Mater. 167 (2018) 115–142, https://doi.org/10.1016/j.conbuildmat.2018.01.143.

[29] D. Snoeck, N. De Belie, Autogenous healing in strain-hardening cementitious materials with and without superabsorbent polymers: an 8-year study, Front. Mater. 6 (2019) 48, https://doi.org/10.3389/FMATS.2019.00048/BIBTEX.

[30] D. Snoeck, Autogenous healing in 10-years aged cementitious composites using microfibers and superabsorbent polymers, Infrastructure 7 (2022) 129, https://doi.org/10.3390/INFRASTRUCTURES7100129, 129. 7 (2022.

[31] V. Cappellesso, D. di Summa, P. Pourhaji, N. Prabhu Kannikachalam, K. Dabral, L. Ferrara, M. Cruz Alonso, E. Camacho, A review of the efficiency of self-healing concrete technologies for durable and sustainable concrete under realistic conditions, Int. Mater. Rev. (2023), https://doi.org/10.1080/09506608.2022.2145747.

[32] S. Al-Obaidi, M. Davolio, F. Lo Monte, F. Costanzi, M. Luchini, P. Bamonte, L. Ferrara, Structural validation of geothermal water basins constructed with durability enhanced ultra high performance fiber reinforced concrete (Ultra High Durability Concrete), Case Stud. Constr. Mater. 17 (2022), e01202, https://doi.org/10.1016/J.CSCM.2022.E01202.

[33] F. Lo Monte, L. Ferrara, Tensile behaviour identification in Ultra-High Performance Fibre Reinforced Cementitious Composites: indirect tension tests and back analysis of flexural test results, Mater. Struct. Constr. 53 (2020) 1–12.

[34] S. Al-Obaidi, S. He, E. Schlangen, L. Ferrara, Effect of Matrix Self-Healing on the Bond-Slip Behavior of Micro Steel Fibers in Ultra High Performance Concrete, Cem. Concr. Compos. ((n.d.)).

[35] M. Davolio, S. Al-Obaidi, M.Y. Altomare, F. Lo Monte, L. Ferrara, A methodology to assess the evolution of mechanical performance of UHPC as affected by autogenous healing under sustained loadings and aggressive exposure conditions, Cem. Concr. Compos. 139 (2023), 105058, https://doi.org/10.1016/J.CEMCONCOMP.2023.105058.

[36] L. Ferrara, M. Cremonesi, M. Faifer, S. Toscani, L. Sorelli, M.A. Baril, J. Réthoré, F. Baby, F. Toutlemonde, S. Bernardi, Structural elements made with highly flowable UHPFRC: correlating computational fluid dynamics (CFD) predictions and non-destructive survey of fiber dispersion with failure modes, Eng. Struct. 133 (2017) 151–171, https://doi.org/10.1016/J.ENGSTRUCT.2016.12.026.

[37] L. Ferrara, M. Faifer, S. Toscani, A magnetic method for non destructive monitoring of fiber dispersion and orientation in steel fiber reinforced cementitious composites-part 1: method calibration, Mater. Struct. Constr. 45 (2012) 575–589, https://doi.org/10.1617/S11527-011-9793-Y/FIGURES/14.

[38] L. Ferrara, M. Faifer, M. Muhaxheri, S. Toscani, A magnetic method for non destructive monitoring of fiber dispersion and orientation in steel fiber reinforced cementitious composites. Part 2: correlation to tensile fracture toughness, Mater. Struct. Constr. 45 (2012) 591–598, https://doi.org/10.1617/S11527-011-9794-X/FIGURES/5.

[39] W.L. Walters, Determination of impact resistance by measurement of coefficient of restitution, (n.d.) .

[40] D. Snoeck, K. Van Tittelboom, S. Steuperaert, P. Dubruel, N. De Belie, Self-healing cementitious materials by the combination of microfibres and superabsorbent polymers, J. Intell. Mater. Syst. Struct. 25 (2014) 13–24.

[41] D. Snoeck, N. De Belie, From straw in bricks to modern use of microfibers in cementitious composites for improved autogenous healing – a review, Construct. Build. Mater. 95 (2015) 774–787, https://doi.org/10.1016/J.CONBUILDMAT.2015.07.018.

[42] G. Weir, S. Tallon, The coefficient of restitution for normal incident, low velocity particle impacts, Chem. Eng. Sci. 60 (2005) 3637–3647, https://doi.org/10.1016/J.CES.2005.01.040.

[43] M. de Rooij, K. Van Tittelboom, N. De Belie, E. Schlangen, in: Self-Healing Phenomena in Cement-Based Materials, 2013, p. 11, https://doi.org/10.1007/978-94-007-6624-2.

[44] D. Snoeck, N. De Belie, Repeated autogenous healing in strain-hardening cementitious composites by using superabsorbent polymers, J. Mater. Civ. Eng. 28 (2015), 04015086, https://doi.org/10.1061/(ASCE)MT.1943-5533.0001360.